Piezoelectric Flexing and Output Voltage of a Microchannel Heat Engine

by

Paul Aquino, B.Eng.

A thesis presented to the

University of Ontario Institute of Technology

in fulfilment of the thesis requirement for the degree of

Master of Applied Science

in

Mechanical Engineering

Oshawa, Ontario, Canada

Abstract

In this thesis, a new model is formulated for a piezoelectric membrane and fluid motion in a microchannel heat engine. A new slug flow model is developed for droplet motion in a circular cross-section channel. The model includes friction, pressure, viscous and thermocapillary forces on the droplet. This thesis examines the concept of a piezoelectric device at one end of the channel to generate electricity from thermocapillary pumping of the droplet within the microchannel. The slug flow model is used to predict the flow energy needed to convert the thermocapillary pumping into electrical energy. A thin membrane design of a piezoelectric device is developed and modelled with the slug flow approximation. The deformation of the piezoelectric membrane is analyzed. The deformation is found to be a function of the air pressure in the closed microchannel and the displacement of the droplet along the microchannel. This was formulated based on the bending of a thin plate (representing the membrane). The displacement relates to the final output voltage of the design. The direct piezoelectric effect was also examined to determine a relationship between the output voltage and induced stress on the membrane by the force of air. Results are presented for a micro heat engine configuration containing a single membrane on one side of the droplet. It was found that the deformation of the membrane and the output voltage were directly proportional to the displacement of the droplet. A relatively small output voltage was gained from a complete cycle of

the droplet. A sensitivity study was performed by varying the channel dimensions along with the dimensions of the piezoelectric membrane. The coupling factor of the piezoelectric membrane was varied to examine its effect on the output voltage. It was found that a larger channel and thinner membrane resulted in a larger output voltage. Materials with a large piezoelectric constant were found to have the largest output voltage, as opposed to those with a lower dielectric constant.

Acknowledgements

I would first like to thank my supervisor, Dr. G. F. Naterer, for his support and understanding. In particular, his recommendations and suggestions have been invaluable in the development of this thesis. I also wish to thank my family for their love, encouragement, and their ability to keep me focused. A special thanks for all my friends and colleagues (especially Adedoyin Odukoya), whose assistance made it possible to complete this thesis. Financial support of this research from the Natural Sciences and Engineering Research Council of Canada, as well as Canada Research Chairs program, is gratefully acknowledged.

Contents

List of Figures

List of Tables

Nomenclature

A	Cross-sectional area (μm^2)
b	Width (μm)
B	Empirical constant
d	Piezoelectric constant matrix, channel height (μm)
D	Electrical polarization, electrical displacement (C/m^2)
E	Electrical field (V/m), Young's Modulus (GPa)
F	Force (N)
G	Shape factor
k	Electromechanical coupling coefficient
I	Inertia (kg/m^2)

l Length (μm)

m Mass (kg)

P Pressure (Pa)

r Radius, distance from the center line of flow (μm)

R Gas constant (J/kgK), channel radius (μm)

t Thickness (μm)

T Temperature (K), stress (Pa)

u Bulk velocity (μm/s)

V Volume (μm^3), voltage (V)

w Deformation (μm)

x Displacement (μm)

Greek

ε Dielectric constant

σ Surface tension (dyn/cm)

μ Viscosity (Pa*s)

τ	Shear stress (Pa)
α	Scalar Coefficient
β	Scalar coefficient

Chapter 1

Introduction

1.1 Background

Microelectromechanical systems, or more commonly called MEMS, are often found as part of sensors, actuators, and electrical and mechanical systems on a silicon substrate through microfabrication technology [1]. The size of a complete MEMS device is typically on the scale of tens of micrometres (1 micrometre = 0.001 mm), with the components on the scale of micrometres. The MEMS market is rapidly growing due to innovation of consumer applications. In the consumer industry, for example, cellular phone technology has a high demand for new advancements in MEMS, as a result of new cellular devices that incorporate many electronic needs.

MEMS devices are found in many different applications from the consumer's perspective. Gyroscopes are now commonly found in many of today's popular entertainment consoles, for example in the controllers for Sony's Playstation 3, which takes advantage of the 6 axes of movement, and Nintendo's Wii. MEMS accelerometers are gaining widespread attention in the wireless market as a result of their usefulness in smart phones. These accelerometers are commonly used because they allow for a change in orientation of the screen, when using the camera feature on a cellular phone to take either portrait or landscape photos. It is also useful in the intuitive operation of the cellular phone itself, when navigating through its varying features.

The MEMS market continues to grow as a result of this high demand from companies for new MEMS technology in their devices. While there was a projected 21.3% drop in overall electronics and wireless devices in 2009, MEMS will have approximately a 6% increase in revenues [1.2]. This indicates the growing potential for the MEMS industry, pending further advancements in research and development.

Besides consumer electronics and wireless devices, MEMS has gained attention in such areas as automotive, industrial, medical, aerospace, and defense. Some key examples of these are accelerometers for collision detection, inkjet printers, and blood pressure sensors. In recent research, MEMS implemented in a biomedical setting has resulted in a miniature heart cell force transducer system

[3]. Other research in this field has led to a MEMS drug delivery device [4], drug testing device [5], and microneedles [6]. MEMS are typically powered by a relatively large power source and so they are restricted by size. For new developments in the field of MEMS, it is important to develop a suitable power source, on the same scale as the system itself, so these systems can become more versatile and further improvements can be made.

Another area of major importance is renewable and sustainable energy. Reliable and renewable sources are needed to sustain the economic growth and move towards a "greener" world. Innovative ways to increase the energy efficiency or recycle energy within a given system are needed so that less is used from fossil fuels. In this way, the carbon footprint can be reduced. With the growing concern for the environment, its future, and the carbon footprints which we leave behind, it is necessary to conduct research to address these problems. With the growing advancements in MEMS and manufacturing, it is useful to take advantage of these technologies for sustainability and the environment. It is the objective of this thesis to examine the utility of a micro heat engine, using MEMS technology, towards a goal of energy sustainability.

To achieve this goal, this thesis will investigate the potential of adding a piezoelectric membrane to the current micro heat engine so that the thermocapillary pumping within the system may be utilized. The current model for the rectangular micro heat engine will be studied and an attempt will be made to

adapt the model to a cylindrical channel with circular cross-section. Once this is complete, a model must be formulated for the piezoelectric membrane. Finally, the two models will be combined to create a new model for the potential output voltage of the system based on the displacement within the channel.

1.2 Literature Survey

The following section is comprised of literature that has been researched for the area of study. It is meant to be a study of the state of the art. However, relations to this thesis do exist between a few of the literature papers and will be clarified where appropriate.

1.2.1 Micro Power Systems

A significant amount of research is being conducted on MEMS at educational institutions and companies. Researchers in France at L'Ecole Normale Supérieure de Cachan have developed a piezoelectric transducer that harvests mechanical vibrations [8]. The transducer measures 20.5mm at its maximum diameter and 630µm in thickness. The device is a combination of both lead zirconate titanate (PZT) and brass, with the PZT resting on a smaller inner diameter of brass. The combination of the brass and PZT design increases the bending moment, which results in maximizing the strain produced by the PZT layer. When the transducer

is placed appropriately, mechanical vibrations are harvested by an oscillating motion in the PZT membrane. The strain is then maximized by the brass layer, which generates the AC voltage across the electrode layer.

Cui et al. [9] at Shanghai JiaoTong University in China have developed a circular piezoelectric actuator for valveless micropumps. They performed an analytical and numerical analysis of the micropumps. The valveless micropumps consist of two diffuser and nozzle elements, a pump chamber, a pump membrane and a piezoelectric layer. The pump membrane itself consists of a passive plate connected to a layer of piezoelectric material by a bonding layer. The main structure starts with a fluid inlet, which is connected to the fluid chamber by a cone shaped structure. It is oriented so the diffuser side is the inlet side. The pump membrane is positioned above the fluid chamber. In between the fluid chamber and the outlet, another diffuser and nozzle structure are oriented in the same way, so they appear in series. The main principle is fluid transport due to the pump membrane, its interaction with the nozzle and diffuser element, and its fluid properties. Fluid enters the chamber as the pump membrane moves to increase its volume. Fluid motion is achieved when there is a sufficient flow resistance at the nozzle end, so when the pump membrane moves to decrease the volume in the chamber, the fluid moves from the inlet to the outlet, and not vice versa. When modeling, the electro-elastic deformation poses a problem. The displacement field and electric field are important issues when performing analytical modeling of the piezoelectric actuator.

Zhang et al. [10] at Tsinghua University in Beijing, China, have developed a new high energy-density micro power generation system. It involves a novel two-stroke cycle micro-piston swing engine (MFPSE) [10]. Researchers have fabricated a prototype for ignition experiments. It is a circular cavity divided into two chambers, with the two chambers being further divided in half by a swing mechanism, with the rotation centre at the centre of the structure. The lower two chambers are used as pre-combustion chambers, with inlet ports and valves for gas inflow. The top two chambers are used for combustion, and they contain one exhaust port in between for waste gases to escape. As combustion occurs in one chamber, compression takes place in the opposing combustion chamber, while gas enters the opposing pre-compression chamber. As the swing moves clockwise, exhaust gases escape the initial combustion chamber and the gas in the initial pre-compression chamber moves in again. As the swing reaches its limit and compresses the gas in the opposing chamber, a spark ignites and the process occurs in reverse. The swing moves counter-clockwise, moving the swing back into its initial position. The prototype was measured at 50mm x 50mm x 35mm and demonstrated successfully at the micro level.

Zhu et al. [11] at the University of Illinois at Urbana Champaign have integrated two micro power systems. The micro-power source is based on a micro-silicon fuel cell and a micro electromechanical hydrogen generator [11]. A microfluidic self-regulating mechanism was shown to be able to control the hydrogen generation with a varying applied electrical load.

Weiss [12] at Louisiana Tech University has developed a new type of micro heat engine with a novel thermodynamic cycle. The concept differs from traditional engines because it does not rely on a rotary based design. The design works under low temperature gradients. A layer of working fluid is contained between two flexible membranes. Heat is transferred through the bottom layer to heat the working fluid. As the working fluid is heated, it expands and evaporates, increasing the pressure in the chamber. This leads to expansion of the top membrane, where the engine performance is determined. At the resonant frequency, this leads to the rejection of heat through the lower membrane, and as a result, compression inside the chamber and a deformation in the reverse direction. A thermal switch was used to control the heat addition and rejection under constant temperature conditions.

Lee and Wilson [14] at the University of Texas, in collaboration with the NASA Johnson Space Center, are investigating a micro power supply using a high-temperature superconductor-magnet bearing. Their micro power supply is constructed from three main components: a flywheel energy storage system, a generator, and a lithium micro battery. Their design helps improve the longevity of the device and the reduction of energy loss from eddy currents and heat dissipation. It has increased the life of the design by implementing a levitated HTS bearing, which is free from friction and mechanical wear. The operation of the motor and generator occurs by means of switching between modes, using pulsed-width modulation and switching between the two functions. The design is promising due

to many factors including size, and power storage to volume ratio. It does not interfere with other MEMS devices, since the vibration in the device is isolated.

There is also increasing interest from the private sector in the field of micro and nano power systems. One such example is the Sierra Pacific Power Company in Reno, Nevada, which improved the electrical performance of a new micro-turbine generator [15]. The micro-turbine generator is a three-phase, 480 volt, 30 kW design. The end result of having these micro-turbine generators is to connect them in series and thus increase the effectiveness of small energy distribution stations.

1.2.2 Micro Fabrication Technologies

A MEMS power generator with transverse mode thin film PZT has been fabricated at the Korea Institute of Science and Technology in Seoul, South Korea [16]. The structure of their power generator is similar to that of a classic cantilever design for piezoelectric actuators. The cantilever beam has layers of a membrane, a diffusion barrier and buffer layer, a piezoelectric thin film layer, a top interdigitated electrode, and an optional proof mass layer. The power generator produces an AC current because of the deflection of the membrane, due to tensile and compressive stresses. The cantilever experiences these changes in tensile and compressive stresses when it is vibrating at the resonant frequency. During fabrication, extra layers were added to the top and bottom of the PZT layer to reinforce the cantilever

and reduce residual stresses. These residual stresses were creating a large bow in the cantilever that was undesirable during fabrication of the cantilever beam. The cantilever apparatus interacts with the electric circuit and storage capacitor via two bonding pads. The researchers have poled the device using traditional methods of heating and poling to 90 V, and cooling with the applied pole. During experimentation, the device produced resultant charges of 4.14 pC per μm of displacement of the tip of the cantilever beam. A maximum charge of 13.2 pC was generated at a displacement of 2.56μm. After they connected the device to the rectifying circuit, results were obtained for the voltage and compared to the applied load. A maximum voltage of 3V was achieved when the load reached 10.1 MΩ. It was found that the voltage decreased with a higher load.

Researchers at the National University of Singapore and California State Polytechnic University have developed a micro-thermophotovoltaic power generator [17]. Their design consists of a micro mixer, cooling fins, photovoltaic cells, filters, and a micro-flame tube combustor. The combustion chamber was constructed of broadband and selective emitting materials. When a gas mixture reacts inside the combustion chamber, the walls of the emitter are heated. Once it is heated to the desired temperature, the wall emits photons that eventually strike the photovoltaic cells. This interaction results in electricity via free electrons. The system is advantageous because of the greater surface area to volume ratio. When compared to a typical system on the macro scale, the surface area to volume ratio was much greater on the micro scale, resulting in a power density of 133.3 W per volumetric

unit, compared to 2 W per volumetric unit on the macro scale. The dimensions of the design are a cylinder of 2cm in length and 0.3cm in diameter. The results of the prototype show that the generator is able to produce 0.92W of power, with a flow rate of gas of 4.2g/h, when the hydrogen to air ratio is 0.9. A 1.45W power output is expected if the photovoltaic cells are upgraded.

At the Korea Institute of Science and Technology in Seoul, Korea, researchers have examined the optimal design of a piezoelectric cantilever, moved by a microbubble in the micro power generator [18]. The micro power generator uses the principle of the piezoelectric effect in conjunction with cantilevers. The cantilever itself is actuated by a microbubble inside the generator. The generator works by varying the temperature differences where the system is located, such as human skin. The microbubble eventually moves up the cantilever, due to these temperature differences, and the cantilever produces electricity due to the deformation of the piezoelectric layer of the cantilever. The researchers found the optimal design of a cantilever for the micro power generator, to harness the maximum amount of electrical output from the deformation of the PZT layer. Varying the force of the microbubble, or changing the shape of the cantilever beam, may improve the resultant electrical output.

At Imperial College, London, Miao et al. [19] examined a MEMS inertial power generator. It works on electrostatic conversion and the application requires functionality under low frequencies of movement. It is divided into three layers,

stacked on top of one another. The bottom layer contains the charging contacts and the stationary plate, the middle layer has the moving plate and conducting suspension, and the top plate has the discharge contacts. Initially, the moving plate is at its lowest point in contact with the charging contacts. A priming voltage is applied during initial startup, which serves as a holding force between the stationary plate and the moving plate. Energy conversion is then achieved when there is enough force from movement, to force the moving plate to drift away from the stationary plate. The stationary plate passes through the flight phase and eventually comes into contact with the discharge studs, to discharge into the load circuit. During this flight time, the voltage in the system rises according to the ratio of initial to final capacitance, as capacitance drops during the flight phase. Their device measures about 2 cm by 2 cm, about the size of a standard quarter dollar. The experiment recorded a resultant output voltage of about 220V, or 120nJ per cycle.

Jiang et al. [20], at the University of Birmingham, UK, developed a micro reciprocating engine for a time multiplexed deep etching process. While conventional designs normally have a circular piston because of fabrication processes, the authors used a square shaped piston as the fabrication technique. The main difference between their design and conventional engines is this square piston and a gear shaft, instead of a crankshaft. The cross-section of the square piston measures 1 square millimeter, while the stroke of the piston is 1.176 mm. Theoretically, with a rotational speed of 5,000 rpm, the engine output is 7.30 mW.

The square shape of the piston creates a problem, concerning leakages. As a result of the square shape, the authors were unable to use O-rings to seal the piston, as traditionally used. Instead, they extended the piston block and etched grooves onto the end, to reduce the pressure leakage.

At the Micro and Nano Systems Laboratory at MIT, Hajati and Kim [21] examined a rectifier-less piezoelectric micro power generator. Unlike previously developed power sources, this piezoelectric micro power generator takes advantage of vibrational energy sources. The system builds upon a type I piezoelectric micro power generator, which is an interdigitized electrode stacked upon layers of piezoelectric material in cantilever form. A mass is attached to the end of the cantilever, to increase the vibrational effect from the base. The new type II piezoelectric micro power generator (developed by Hajiti and Kim) incorporates many aspects of the type I into a pie-shape structure. Type I micro generators are placed in a circular pattern shape, converging onto the same mass at the centre. They are also connected by an outer rim. With the type II PMPG, each beam circling the mass encounters a compressive and tensile strain when a deformation occurs on the entire structure. During deformation, the beam bends and experiences tensile strain at the top of the front of the beam, while the end top of the beam experiences compressive strain. These two strains converge at the midpoint of the beam, where no tensile strains are present. The reverse occurs at the base of the beam, where compressive strains exist at the front, and tensile strains exist at the end. These are a result of the beam being fixed at both ends, by

either the structure or the mass. The beams also undergo a tensile strain, as a result of stretching. As the mass moves, the beam must follow and stretch, as it has no other way to deform to account for the displacement, horizontally. This stretching strain produces the same sign charges at the electrodes. The prototype is very small and about the size of a nickel.

1.2.3 Micro Engines

At Carleton University, Canada, Ono et al. [22] have examined the use of piezoelectric films for airflow monitoring, to monitor breathing patterns during sleep. Knowing the condition of a person's sleep aids them in diagnosing sleeping disorders, by measuring cessations of breathing during sleep. The traditional way of performing these tests is expensive and not readily available. To alleviate this problem, Ono et al. [22] developed a piezoelectric membrane sensor and technique for breathing monitoring. Their design incorporates a piezoelectric membrane, to bend in accordance with incoming air pressure, much like the traditional cantilever beam model. The device is attached to the face in areas where breathing occurs, below the nose and the mouth. It consists of a circuit, top electrode, piezoelectric film, and metallic substrate. The active components of the design measure 20mm by 4mm. The authors were able to measure and relate the output voltage of the piezoelectric sensor to airflow speed. They used a charge amplifier to amplify the

electric charge signal from the sensor. This has a high flexibility, due to the porosity inside the film and relatively small thickness of the substrate.

Piechna [24] at the Institute of High Performance Computing in Singapore, has developed an improved micro-combustor design, compared to the original micro gas turbine engine at MIT [24]. A goal was to stabilize the combustion in the micro gas turbine engine by adding a wafer layer of microchannel. The flame burns in the bottom and top recirculation jackets of the engine, resulting in a higher temperature at the engine walls. These higher temperatures lead to a shorter life span. To alleviate this problem, Piechna [24] stabilized the combustion so that the flame burns only in the combustion chamber. Originally, the bottom recirculation jacket contained a microchannel that led to the flame holders. With microchannels spanning along the perimeter and inwards, gas enters the top microchannel and mixes with air. The mixture then flows towards the right side and eventually to the bottom recirculation jacket. After the recirculation jacket, the air and gas mixture flows inwards to a combustion chamber located at the center, comparable to a pinwheel. To stabilize the combustion and prevent the flame from retreating into the bottom recirculation jacket, Piechna [24] added a microchannel to increase the distance from the bottom recirculation jacket, to the centre where combustion takes place. The extra microchannel was placed just after the bottom recirculation jacket, oriented so the flow moves around a bend of 180 degrees, into the combustion chamber. The addition of this microchannel allows reduction of space of the engine. The improved design measures 2.1cm by 2.1cm by 0.38cm.

A feasibility study of a wave disk micro-engine has been conducted by Beeby et al. [25] at the Warsaw University of Technology in Poland. Micro turbine engines normally have a relatively low efficiency, despite their high power to weight ratio. This is due to similar flow velocities, as compared to larger scale engines, but they are susceptible to greater wall effects as a result of the size of the engines and channels. To counteract this, the authors have proposed a wave disk micro-engine with single-stage or two-stage compression, with only one rotating part, the compression and decompression disk. The engine consists of the single rotating part and comprises many channels for air and gas mixtures, along with the associated combustion chambers and inlet and outlet ports.

Vibrational energy harvesting is another active area of research for MEMS. Bardaweel et al. [26] developed a micro electromagnetic generator for vibration energy harvesting. The intention is to harvest energy from low frequency applications. The size of the design is about $0.1cm^3$. The design is based on a larger scale concept and comprised of four high energy destiny sintered, rare earth neodymium, iron boron magnets, a beam to attach the magnets, zintec keeper, tungsten mass, copper coil, and a Tecatron GF40 base. The operation of the design is to convert vibrations into electrical energy via a kinetic energy generator. The energy is converted by an electromagnetic mechanism, or by a direct piezoelectric effect. The predicted power output is 185 mVpk for a magnet size of 2.5mm x 2 mm x 1.5mm.

Lee et al. [28] developed a micro combustion-thermionic type of power generation. It builds upon the shortcomings of previously described micro combustion power generators. By comparison, mechanical engines have moving parts and are more costly to fabricate, whereas the thermionic combustion device requires no moving parts, and MEMS fabrication techniques are readily available. Thermionic power generation is based on electron emission from an emitter to collector. The emitter is a hot cathode where electrons gain thermal energy to overcome an energy barrier. When they overcome this barrier, they move to the collector, a cold anode. The anode and cathode are connected by a circuit, so the Fermi potential difference between the two electrodes produces the output voltage. The research study found that certain faults need to be overcome, such as electron cloud formations in the gap. The experimental results showed an overall power output of about 1μW with an overall efficiency of about 10^{-6} for the subsystem. This is relatively low (typically 1-10%) and it is proposed that the efficiency can be improved at higher temperatures. It is expected that the efficiency of the system discussed in this thesis will also be relatively low since it is still theoretical and in early stages of development. After significant research has been conducted, it is expected to be about 1-10% [50].

Martinez and Chowdhury [29] at the University of Birmingham have designed and fabricated a micro Wankel engine using MEMS technology for the replacement of batteries by micro engines. The micro Wankel engine is similar to the traditional Wankel engine, although the authors have modified the housing

curve to remove the compression stage of the Otto cycle. The entire assembly is 15 mm by 12.2 mm by 3 mm. It has a power output of 12W, when operating at 17,000 rpm. The authors have modified the housing by moving one of the curves inwards, to remove the compression phase while keeping the expansion phase.

Toriyama et al. [30] developed a two-stator MEMS power generator for cardiac pacemakers. The operation of the power generator relies upon bodily functions. Voltage is produced by the movement of the thorax during breathing. It consists of a shaft, planar copper coil, magnet, substrate, contact pad, and rotor. Initially the rotor is at rest, at an initial position, then as one breathes, it forces the rotor to move its resting position and oscillate until coming to a stop at a different position. There is a changing magnetic flux that passes through the planar coil to induce the resultant voltage. As a result of breathing, the output voltage is generated in peaks. Instead of a semicircular rotor, a circular rotor was used with a destabilizer. After obtaining results experimentally from a prototype, the authors achieved 390 mW of power, and up to 9 volts RMS.

Mitcheson et al. [31] developed a thermoelectric micro power generator that utilizes a self-standing polysilicon-metal thermopile. For this to produce power output, the device relies on a temperature difference between the hot and cold contacts, as well as thermal isolation and the Seebeck effect. The structure contains an Si substrate, hot contacts, heat absorber, thermocouple, cold contacts, and an insulating layer. Radiated heat from a source is transferred from hot contacts to cold contacts, via a thermopile and insulated membrane. The authors

found that the efficiency is low due to the heat absorber being placed on the same plane as the cold contacts. In their improved design, they developed a self standing structure that eliminates the insulated membrane, thus the only heat transfer from the hot contacts to the cold contacts is through the thermopile. After completing an experimental prototype, the authors demonstrated results of 100-120 μV for the Seebeck voltage and showed this occurs at the minimum deflection.

Carotenuto et al. [32] at Imperial College, London, developed a MEMS electrostatic micropower generator for low frequency operation. The device is based on a motion-driven electrical generator, consisting of a spring-mass-damper system. A spring-mass-damper system is not feasible in non resonant, low frequency operation since the force of the spring may overcome the force applied to the mass. The authors used the Coulomb force to harvest non-resonant, low frequency vibrations, with the Coulomb force, the spring constant is zero and the damping force is constant and opposes the motion between the mass and frame. This type of damping force be employed as an attractive force between the parallel capacitor plates, or by parallel sliding plates. Instead of gaining an output voltage when the system matches a certain resonant frequency, their proposed solution converts energy when the acceleration of the frame is greater than the damping force per unit of mass. After fabricating a prototype and undergoing experimental studies, the authors obtained an overall resultant voltage of 220V.

1.2.4. Piezoelectrics for MEMS

Piezoelectric systems have useful applications in MEMS. At the Università di Salerno in Italy, researchers developed a low voltage piezoelectric micro motor using a thin circular membrane [33]. The motor consists of a permanent magnet rotor, steel axis, and a piezoelectric membrane, all with a common centre axis. The cylindrical magnet is pressed into the top surface of the axis by magnetic forces. The piezoelectric membrane is used to excite a travelling wave, due to the direct piezoelectric effect to produce a natural flexural vibration. Up to 4,000 rpm angular speed without a load torque at an excitation amplitude of 18 were measured.

Kulah and Najafi [34] developed a micro power generator with planar coils on parylene cantilevers. The design consists of cantilevers in series that contain coil turns connected externally by a circuit to produce an output voltage. Their design incorporates a magnet at the ends of the cantilevers, but not in direct contact. The output voltage is a direct result of the motion between the magnet and resonating cantilevers. The authors selected Parylene C as the cantilever material which is more flexible than commonly used silicon. A square array of cantilevers was constructed like the type II PMPG, except that the cantilevers are arranged around the perimeter of a square, and unattached towards the centre where there is an

opening for a magnet. A maximum output voltage of 8.75 mW at a frequency of 5.135 kHz was measured. The prototype design was 9.5 mm by 8 mm by 5 mm.

Lu et al. [35], at the University of Michigan, have developed an electromagnetic micro power generator for low-frequency environmental vibrations. The application of their device will convert low frequency environmental vibrations to a higher frequency. Another configuration is a square arrangement of cantilever beams surrounding a magnet. The magnet in this case has two pieces, one for electromagnetic generation, and the other for frequency conversion. The cantilever beam contains a magnetic tip for more attraction between the cantilever and magnet. In this way, the beam is able to resonate at its resonant frequency. As a result, coil size and beam deflection are reduced. Also, there is an increase of efficiency in energy conversion. The authors obtained a maximum power of 2.5 μW/cantilever and a maximum voltage of 150 mV. The author also analyzed micro piezoelectric power generators for micro-electromechanical-system applications. The authors discussed the principles of piezoelectric energy conversion.

At Washington State University, Whalen et al. [36] developed a resonant micro heat engine, called the P^3 micro heat engine. Their design incorporates a working fluid, piezoelectric membranes, microchannel, and compression and expansion work modes. Their design consists of a vapor bubble contained inside a microchannel that is closed at both ends. At the top and bottom of the microchannel, piezoelectric membranes are inserted. Their process has 4 main stages to complete one cycle: heat addition, expansion, heat rejection, and

compression. During phase 1, heat is transferred to the working fluid through a thin membrane. The volume inside the cavity increases due to the increase of pressure and temperature. This increase in pressure forces the membrane to flex outwards, thus producing a direct piezoelectric effect. Heat is rejected and the system returns for a brief moment to its initial state. As heat is rejected, it gains momentum in the downward direction, which results in a compression stage that forces the bottom membrane to flex inwards. The cycle is then complete, and heat is then added again. In terms of fabrication, the authors used lead zirconate titanite as the piezoelectric material. Each membrane is constructed with silicon and one membrane containing a thin film piezoelectric generator, and the other containing a resistance heater. The micro heat engine is 10 mm by 18 mm on a wafer. The cavity is about one sixth the total size and it is situated in the middle. During testing, the researchers tested the micro heat engine to resonate at its resonant frequency of 240 Hz. During this time, samples were taken at 1,000 Hz and the output was found to be between 63 and 135 mV.

1.3 Thesis Overview

This thesis investigates a new type of micro heat engine, using a cylindrical channel with circular cross-section and the addition of a piezoelectric membrane. The heat engine operates on the principle of mechanical to electrical energy conversion via thermocapillary pumping of an enclosed droplet. Transport

phenomena of thermocapillary pumping and droplet motion inside the microchannel during power generation are examined. In addition, piezoelectric membrane dynamics will be examined to generate electricity from the mechanical work of the moving droplet. The analysis of droplet motion and piezoelectric membrane dynamics represents a new and novel contribution of this thesis, beyond past studies reported in the literature.

Chapter 2 develops a formulation of the droplet motion in a closed microchannel. Chapter 3 analyzes flexing of the piezoelectric membrane due to the droplet motion. The output voltage form the flexing membrane is then analyzed in Chapter 4. Results and discussions are presented in Chapter 5, followed by conclusions and recommendations in Chapter 6.

Chapter 2

Formulation of Droplet Motion

In chapter 1, an introduction to micro power systems was presented. This chapter examines thermocapillary droplet pumping inside a closed microchannel. It develops a model for the motion of the droplet, when it moves back and forth inside the channel. When the droplet is heated and cooled in a cyclic pattern, the droplet oscillates. As the cyclic heat source heats one region of air, there is an increase of pressure in the system. The main transport mechanism of the droplet is induced by a difference in surface tension, with respect to the receding and advancing edges of the droplet. The following sections will examine the effect of temperature change on the system, and additionally the three main forces affecting the droplet motion inside the microchannel. A model is formulated for the purpose of predicting flow behavior of the droplet, and determining the pressures and resultant forces, to predict the droplet displacement and velocity, leading to power output (discussed in next chapter).

2.1 Problem Description

Consider the processes of thermocapillary pumping (TCP) of a droplet in a closed microchannel with a piezoelectric membrane. Thermocapillary pumping involves droplet motion within a closed-ended microchannel, due to varying temperatures and pressures on either side of the droplet. The placement of a piezoelectric membrane occurs at either end of the microchannel.

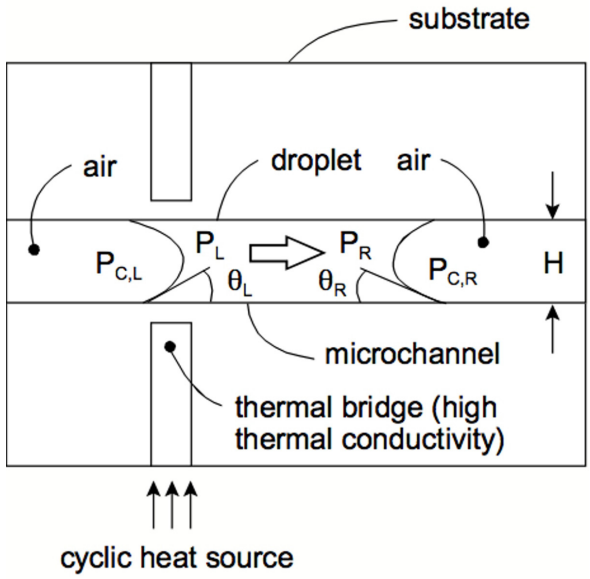

Figure 2.1: Basic Concept of Droplet Motion with TCP

The thermocapillary pumping inside the microchannel occurs due to an applied temperature difference between the opposing ends of the microchannel. Consider a heat source that cycles on and off on one side of the microchannel, as depicted in Fig. 2.1. A single droplet is contained inside the microchannel to initiate the pumping action. As the temperature increases in the left side of the channel,

the droplet moves from left to right. Due to surface tension changes, receding and advancing droplet angle changes, and thermocapillary pressure changes across the droplet, a pressure difference forms inside the droplet. As the back end of the droplet is heated, the surface tension and receding meniscus decreases which results in a decreased capillary pressure. During this stage, the contact angle between the receding end and the wall decreases. To compensate for the change in droplet form, the contact angle between the advancing end and the wall increases which decreases the interfacial capillary pressure and increases the internal pressure in the advancing end of the droplet. This internal pressure difference inside the droplet is the main transport mechanism for the direction in which the droplet moves as the droplet compensates for changes. As the droplet moves from left to right, the pressure in the right enclosure increases. When the heat source is turned off, or removed, the system will move back to an equilibrium position. This cycle of heating and cooling produces the thermocapillary pumping motion. The thermocapillary pumping can be harnessed for a useful application. The pumping action produces a pressure at both ends of the microchannel, but to no use unless there is further energy conversion. The new design in this thesis will replace these ends with a system that would convert this droplet work into useable energy, in the form of an electrical potential, via a piezoelectric membrane.

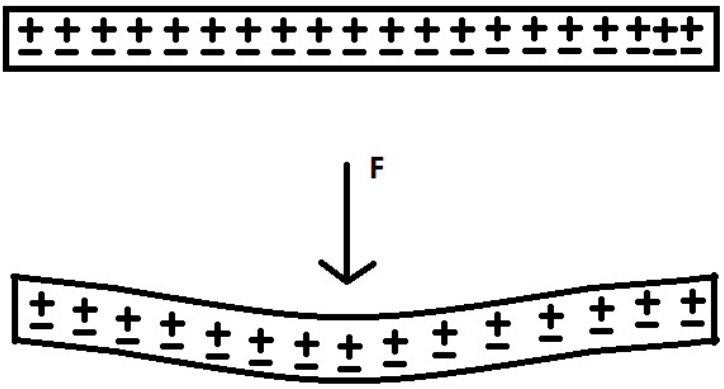

Figure 2.2: Illustration of displacement of charge centres

Piezoelectricity is the phenomenon by which a material will produce an electric charge due to imposed mechanical stress or vice versa. The direct effect of piezoelectricity is when the electric charge is the result and the inverse effect is when there is a mechanical stress produced [7]. For example, a 1,000 V/cm field applied between the ends of a quartz rod produces a strain of 10^{-7}. The reverse effect is possible for generating an equally large field by applying a relatively small mechanical stress. These electrical fields are a result of the microscopic displacement between charge centers within the material. Piezoelectric materials are crystals. As a result, a stress applied to a crystal will increase or decrease the distance between centers of positive and negative charges. This results in a net polarization, and one can then measure this as an open circuit voltage. The usage of piezoelectricity is diverse, as there are many applications. Piezoelectric membranes

can be found in various types of MEMS sensors and actuators. They are used in sensors because they can produce a voltage under stress, which can be measured and converted into a useful output. As an actuator, an electrical field can be applied to produce a deformation, at precisely the required value when calculating the voltage needed.

The material can be made piezoelectric in any direction by poling the crystals in the material. This process of creating a piezoelectric material to the required state involves heating to an elevated temperature, while exposing it to a strong electric field. The domains nearly aligned with the field grow at the expense of others, and additionally grow in length in the direction of the field. The field is then removed and the dipoles are locked into a desired position. The effect of piezoelectricity can be removed from the material by the same method. If the material is exposed to a strong electric field in the opposite polarization, it is possible that the effect will be negated. Likewise, if heated to a high enough temperature specific to the material, the Curie point or Curie temperature, the same will happen.

In piezoelectricity, one can find the resultant electrical polarization in a material due to the applied mechanical stress, as follows,

$$D = dT + \varepsilon E \tag{1.1}$$

where D is the resultant electrical polarization, d is the piezoelectric coefficient matrix, T is the stress matrix, ε is the electrical permitivity matrix, and E is the

electrical field. The terms d and ε are specific to the type of piezoelectric material. The units for electrical displacement, piezoelectric constant, stress, permitivty, and electric field are C/m^2, C/N, N/m^2, F/m, and V/m, respectively. In this thesis, no electric field will be applied, and only stress will be examined with the piezoelectric material. Therefore, the 2nd term with the electric field will be assumed zero. Thus, the equation in full form becomes:

$$\begin{bmatrix} D_1 \\ D_2 \\ D_3 \end{bmatrix} = \begin{bmatrix} d_{11} & d_{12} & d_{13} & d_{14} & d_{15} & d_{16} \\ d_{21} & d_{22} & d_{23} & d_{24} & d_{25} & d_{26} \\ d_{31} & d_{23} & d_{33} & d_{34} & d_{35} & d_{36} \end{bmatrix} \begin{bmatrix} T_1 \\ T_2 \\ T_3 \\ T_4 \\ T_5 \\ T_6 \end{bmatrix} \tag{1.2}$$

The superscript for the electric polarization indicates the electrical polarization axis by which it is defined, where 1 is the X-axis, 2 is the Y-axis, and 3 is the Z-axis. The terms for stress T_1-T_3 indicate the normal stress for axes 1-3, while T_4-T_6 indicates the shear stresses on axes 1-3.

The electromechanical coupling coefficient k is a measure of the amount of energy transferred from electrical to mechanical energy, or vice versa, and is specific for each material as well as the geometry and oscillation mode. It is related to the energy by the following equation:

$$k^2 = \frac{energy\ converted}{input\ \ energy} \tag{1.3}$$

2.2 Temperature Changes in the System

At an equilibrium temperature, the system is at rest. In this thesis, the droplet's working fluid is water and the gas at either side of the channel is air. Heat is supplied, and the droplet moves in the direction opposite of the side of increasing temperature, until a maximum distance is reached based on a force balance. As the temperature source is removed, a cooling period begins. The droplet then moves back to its original position. Instead of a period of cooling, a secondary heat source can be applied to the opposing side of the channel, allowing the droplet to traverse the length of the microchannel in the opposite direction. This section will examine changes in temperature with respect to heating and cooling of the various areas of the microchannel.

As the cyclic heat source changes in temperature, there is a transfer of heat between the walls of the microchannel, the air on one side of the droplet, and the droplet itself. As the temperature is increased, the walls of the microchannel increase in temperature, which in turn increase the temperature of the air in one side of the microchannel. Pressure increases in the enclosed air, while pressure remains unaffected at the other end of the microchannel initially. The heat also transfers to the droplet itself resulting in a pressure increase in the receding edge of

the droplet and a pressure decrease in the advancing edge. The heat source affects the entire height of the channel.

Cooling of the microchannel begins when the cyclic heat source is turned off. The cooling stage is passive, whereas the heating stage was active. During the heating stage, the cyclic heat source creates a temperature increase. In the cooling stage, instead of a temperature difference provided by the heat source, the droplet and air chambers interact with the surroundings to release heat provided by the heating period previously. Thus the heating and cooling stages are different, and they also require varying amounts of time.

The duration for the heating period is controlled as a function of the desired distance travelled for the droplet in the microchannel. In comparison, the duration of the cooling period is determined by the heat flow between the droplet and air with their surroundings. The factors determining this are the surrounding temperatures and conditions, and magnitude of heat input, among others which can be manipulated based on the nature of application of the system.

2.3 Droplet Displacement

Heating and cooling affect the droplet displacement. Also, there are three main forces, either assisting or resisting the movement of the droplet, inside the channel. These are the pressure force of air, thermocapillary force, and frictional force. The sum of these forces provides the net force that is used to describe and predict the motion of the droplet according to Newton's Second Law.

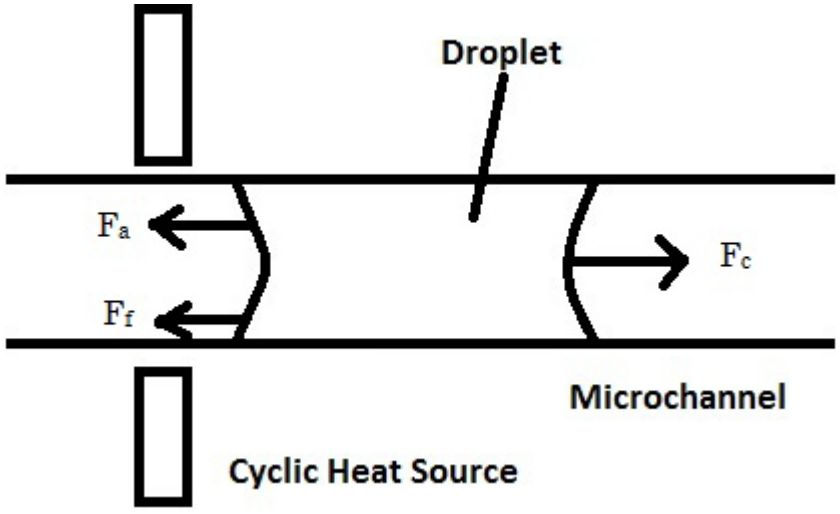

Figure 2.3: Force diagram

2.3.1 Force of Air

During the heating and cooling periods, there is a change of pressure in both sides of the microchannel. This change in pressure creates a net force of air on the droplet. As the cyclic heat source provides heat to one side of the channel, the air

contained on that side expands, modeled after the ideal gas law. Since the channel is a closed-ended channel, the opposing side of air is also affected. As pressure increases and the air expands on the receding side of the droplet, air in the advancing side of the droplet is compressed due to the motion of the droplet. This expansion and compression of gases has an effect on the motion of the droplet that must be considered. Modeling from the ideal gas law, the force can be approximated from

$$PV = mRT \tag{2.1}$$

where P is the pressure, V is the volume, m is the mass of gas, R is the specific gas constant for dry air equal to 287 J/kgK, and T is the temperature of the gas. Re-writing in terms of pressure,

$$F = PA \tag{2.2}$$

$$P = \frac{mRT}{V} \tag{2.3}$$

Force is directly proportional to pressure over a specified area, leading to

$$F_a = \frac{AmRT}{V} \tag{2.4}$$

where A is the cross sectional area of the channel. There are two forces of air present and the resultant force is obtained as follows,

$$F_a = AR\left[\left(\frac{mT}{V}\right)_L - \left(\frac{mT}{V}\right)_R\right] \tag{2.5}$$

where the subscripts L and R denote the side of the channel (left and right).

2.3.2 Thermocapillary Force

In this thesis, water is selected as the droplet working fluid. A desired working fluid for the system has a high surface tension to coefficient of friction ratio. Selecting water as the working fluid will be briefly explained below.

One of the reasons for motion of the droplet is the phenomenon of capillary action and the resulting thermocapillary force. The thermocapillary force is a result of temperature differences across the droplet, and like capillary action, the resulting surface tension. The surface tension at either edge of the droplet can be found with the following equation [48]:

$$\sigma = A - BT \tag{2.6}$$

where A and B are property constants of 75.83 dyn/cm and 0.1477 dyn/cmK, respectively, for water. In the equation, there are no geometrical factors.

$$F_c = \left(P_{c,R} - P_{c,L}\right)A \tag{2.7}$$

Eq. (2.7) defines the thermocapillary force, denoted by the subscript "c" for capillary. The two terms in the brackets are the individual pressures in the droplets at both the receding and advancing edges. The subscripts R and L indicate the side of the droplet (right and left).

$$P_c = \frac{G\sigma\cos\theta}{d} \tag{2.8}$$

The surface tension is then used to find the capillary pressure in Eq. (2.8). It follows that the thermocapillary force equation is found in the following form,

$$F_c = GA\left[\left(\frac{\sigma\cos\theta}{d}\right)_R - \left(\frac{\sigma\cos\theta}{d}\right)_L\right] \tag{2.9}$$

where σ is the surface tension, A is the cross sectional area, d is the channel height, θ is the contact angle between the receding or advancing edge of the droplet and the microchannel wall, and G is a constant based on the geometry of the microchannel profile. The angle θ is assumed to be 0, due to an approximation of the droplet as slug flow. The value of G in this case is 4 for circular microchannels.

2.3.3 Frictional Force

The frictional force is modeled by a steady state velocity profile for Poiseuille flow within the droplet in [48]. The shear stress on the droplet was multiplied by the

area between the droplet and channel interface to give the following equation for a rectangular channel:

$$F_f = \frac{12}{d}\mu \Delta x b u_b \tag{2.10}$$

where b is the channel width and u_b is the bulk velocity of the droplet. To develop this equation for a cylindrical channel with circular cross-section a Hagen-Poiseuille model will be used. For a fully developed Hagen-Poiseuille flow [49],

$$u = \left(-\frac{\partial P}{\partial z}\right)\frac{1}{4\mu}\left(R^2 - r^2\right) \tag{2.11}$$

The bulk velocity can be determined from Eq. (2.11) as follows,

$$u_b = \frac{R^2}{8\mu}\left(-\frac{\partial P}{\partial z}\right) \tag{2.12}$$

The second term in this equation is assumed to have a constant value for a given time step. To find the frictional force, the shear stress on the droplet from the wall must be multiplied by the droplet interface contact area with the wall. The shear stress at the wall is given by [49]

$$\tau_{wall} = \frac{4\mu u_b}{12} \tag{2.13}$$

Considering a cylindrical channel with circular cross-section for the droplet and wall interface, one multiplies the resultant equation with the shear stress on the wall for the droplet, yielding

$$F_f = \left(\frac{4\mu u_b}{12}\right)\left(2\pi R^2 \Delta x\right) \tag{2.14}$$

$$F_f = \frac{2}{3}\mu\pi R^2 \Delta x u_b \tag{2.15}$$

where μ is the coefficient of friction, R is the radius of the channel, and Δx is the length of the droplet.

2.3.4 Droplet Motion

The movement of the droplet depends on the forces of friction, air force, and thermocapillary force. Both the forces of air and friction are resistance forces, as friction works against the movement of the droplet along the microchannel wall, and the force of air next to the advancing edge of the droplet deters it from moving further without a larger opposing force. The thermocapillary force is the force which assists movement of the droplet in the direction of motion. Thus, the thermocapillary force must be greater than the sum of both the air force and the frictional force. This can be observed by the net force on the droplet as follows,

$$F_{net} = GA\left[\left(\frac{\sigma\cos\theta}{d}\right)_R - \left(\frac{\sigma\cos\theta}{d}\right)_L\right] + AR\left[\left(\frac{m_a T_a}{V_a}\right)_L - \left(\frac{m_a T_a}{V_a}\right)_R\right] + \left[\frac{2}{3}\mu\pi R^2 \Delta x u_b\right] \quad (2.16)$$

The net force on the droplet can be found after setting initial conditions. This is used to describe and predict the velocity and movement of the droplet by use of Newton's Second Law. By temporal integration over a discrete time step, the velocity and displacement of the droplet become

$$u_{i+1} = u_i + \frac{F\Delta t}{m} \quad (2.17)$$

$$x_{i+1} = x_i + u\Delta t \quad (2.18)$$

where m is the mass of the droplet and the subscript i denotes the given time step.

This chapter has presented an approximate model of the droplet velocity and displacement, based on friction, pressure and thermocapillary forces acting on the droplet. It has assumed a fixed end wall in the closed microchannel. In the next chapter, a flexing membrane at the end of the channel is examined. This aims to convert flow work of the droplet to electricity, as a new type of micro heat engine in the microchannel.

Chapter 3

Formulation of Flexing Membrane

This chapter develops a new concept for the micro heat engine. It describes the addition of a flexible piezoelectric membrane to the end of the microchannel. This addition of the piezoelectric membrane completes the micro heat engine for electricity generation. The micro heat engine has itself no way of converting the mechanical pumping action of the droplet into electricity. The direct effect of piezoelectricity is the production of an electric field or voltage when a material is flexed under a mechanical stress. In this way, it becomes possible to harness the pumping action of the droplet and convert it to usable electrical energy.

The phenomenon of piezoelectricity has been briefly explained in an earlier chapter explaining the relationship between the electric field and mechanical stress. This mechanical stress is normally in the form of bending when the material is a

thin square film or part of a cantilever design. Developing a predictive model for a piezoelectric membrane can be challenging, especially with certain geometries of membranes. In this chapter, a new model will be developed to show how the membrane will interact with the system. It is assumed that the configuration of the membrane on the microchannel will not interfere with the associated circuitry of the voltage created from the piezoelectric membrane. The configuration of the micro heat engine, material, and membrane deformation will be examined in the following sections.

3.1 Configuration of the Micro Heat Engine

Placement of the membrane is a key issue with the heat engine, in order to maximize the effectiveness of the piezoelectric membrane.

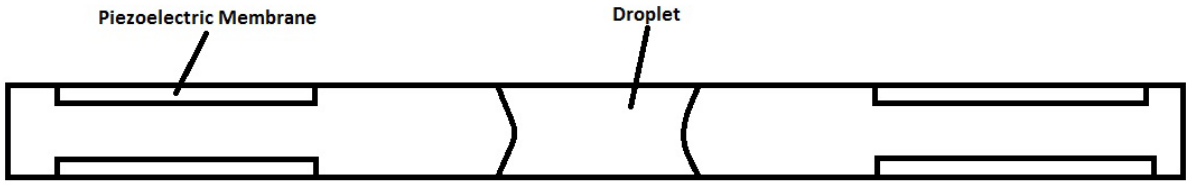

Figure 3.1: Configuration of the piezoelectric membrane

For the piezoelectric membrane in the micro heat engine, the membranes could be placed on either side of the channel in pairs. Fig. 3.1 shows this configuration in terms of the droplet and air spaces in the closed microchannel. Specifically, the membranes are located at the top and bottom of the microchannel on either side. This allows the micro heat engine to make use of the pumping action in both directions. As the droplet moves from left to right, the membranes on the right side would flex outwards, due to air pressure in the right chamber. At the same time, the membranes on the left side displace inwards as pressure decreases in that side of the chamber. The droplet would then complete its cycle by moving right to left, when the opposite deformations occur in the membranes.

Piezoelectric materials are made of many crystals that are aligned and poled in certain directions. Usually the positive poled axis is aligned in the z direction.

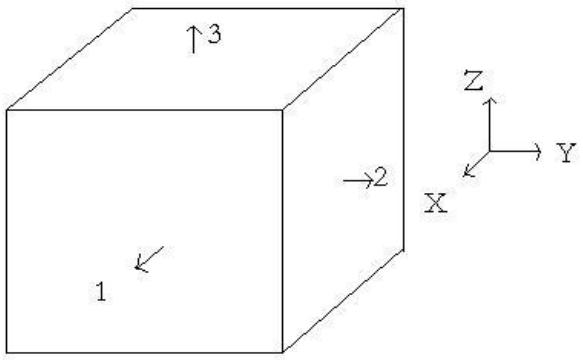

Figure 3.2: Illustration of a piezoelectric crystal

There are various locations where the membrane can be placed. As Fig. 3.1 shows, the top and bottom of the microchannel is one configuration that is commonly used when piezoelectric membranes are employed. From the matrix in Eq. (1.2), the d_{31} term is used to calculate the output voltage. The other terms in the matrix are mostly zero but may differ as each material has a specific matrix. The z direction is the axis of interest. Fig. 3.2 is an illustrated representation of a piezoelectric crystal where the numbers 1, 2, and 3 indicate both the stress and axis.

The configuration allows for full functionality of the membrane. If the membrane is placed at the ends of the microchannel, the direction from which the mechanical stress is switched, and the d_{31} term, may no longer be useful. Instead, the d_{33} term would be used to calculate the output voltage. Furthermore, the shape of the membrane would change, along with greater complexity of the problem. Deformations of circular membranes are more complex problems involving the interaction of the domains in three axes. Numerous studies have been conducted on bending of circular plates. Challenges occur during fabrication also arise when implementing a circular membrane. At the micro scale, using techniques to attach a circular membrane, 1 μm in diameter, to the end of the channel, will prove very difficult. In comparison, attaching a rectangular membrane to the channel is easier, as one can utilize the larger space of length of the microchannel, which measures about 2 mm.

3.2 Piezoelectric Materials

An important step in the addition of a piezoelectric membrane to the microchannel is determining the most suitable material for this purpose. There are numerous materials that exhibit the piezoelectric effect, but some are more suitable for this application than others. The purpose of the membrane is to exhibit the direct effect of piezoelectricity, as opposed to the reverse effect, the deformation of the piezoelectric material when an electric field is applied. There are specific properties of piezoelectrical materials that have importance in this regard.

Material	Dielectric Constant	Young's Modulus (GPa)	Density (kg/m^3)	Coupling Factor	Curie temperature (K)
ZnO (Zinc Oxide)	8.5	210	5600	0.075	-
PZT-4 (Lead Zirconate Titanate)	1300-1475	48-135	7500	0.6	365
PZT-5 (Lead Zirconate Titanate)	1730	48-135	7750	0.66	365
Quartz	4.52	107	2650	0.09	-
Lithium Tantalate	41	233	7640	0.51	350
Lithium Niobate	44	245	4640	-	-
PVDF (Polyvinylidene Fluoride)	13	3	1880	0.2	80

Table 3.1: Properties of piezoelectric materials

Selected properties of piezoelectric materials can be found in Table 3.1. Among these properties, the most relevant are the dielectric constant, the coupling factor, and the Curie temperature. The Curie temperature is the critical temperature at which the piezoelectric material will become depolarized. During the fabrication process, poling occurs when the temperature of the material is elevated. The domains are poled when heat is removed and the material is cooled. Thus, if the material is heated to a high temperature to which it is fabricated, the material would become depolarized. This is important for the application of the micro heat engine. At a higher temperature, the system performance increases, but it may not be able to operate due to the piezoelectric limitations. The other two properties of interest are the dielectric constant and the coupling factor. As investigated further in chapter 4, the following relation holds for the output voltage,

$$V = \frac{D_3 t_{piezo}}{\varepsilon} \tag{3.1}$$

where V is the voltage, D is the electrical polarization, t is the thickness of the piezoelectric stack or membrane, and ε is the dielectric constant. From the equation, the permittivity is inversely proportional to the output voltage. Thus, a good material in this case will require a smaller dielectric constant than average.

The coupling factor is a ratio of the energy converted to the energy input. It is a parameter of the efficiency of the material to convert the energy into the desired output, whether it is a resultant voltage or a deformation due to the added electrical

field. In the case of the micro heat engine, it is a key point in choosing a material that will convert the energy efficiently.

3.3 Deformation of the Membrane

Piezoelectric material output may differ when the material is deformed. The shape and size of the membrane also has a role when determining the resultant output after a deformation. Rectangular membranes are common in MEMS devices that use piezoelectric membranes or thin films. This is due to the ease of implementation and fabrication, as opposed to circular shapes. To model the flexure of the membrane, there are certain assumptions to be made. In the case of a square membrane, it is assumed that it is fixed at the edges and the applied load is distributed two-dimensionally. The stress on the square membrane is highest in the center, and at the midpoints of all opposing edges.

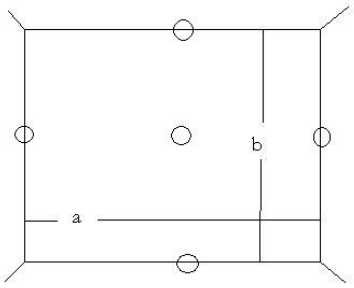

Figure 3.3: Illustration of a square membrane and stress locations

Fig. 3.3 shows an illustration of an approximation where the maximum stresses occur and the dimensions of the rectangle a x b. The values of interest are the maximum displacement of the center and the maximum stresses at the center and edges. The bending of a uniform rectangular plate with distributed loading follows a set of governing equations that describe the maximum displacement and stresses at the center of the diaphragm and midpoints of the edges. These are given by

$$w_{centre} = \frac{\alpha p b^4}{E t^3} \tag{3.2}$$

$$\sigma_{\max} = \frac{\beta_1 p b^2}{t^2} \tag{3.3}$$

$$\sigma_{centre} = \frac{\beta_2 p b^2}{t^2} \tag{3.4}$$

where α and ß are constants, the length to width of the rectangle, p is the load applied, t is the thickness of the plate, and E is the modulus of elasticity for the material. The variable α is dependent on the magnitude of the ratio between the sides a and b of a rectangle. The variable ß is a factor dependent on the location of a point in the in the x or y axis, the subscripts 1 and 2 representing this respectively [47]. Table 3.2 shows examples of values for α and ß as they change with respect to the ratio of a to b.

a/b	1.0	1.2	1.4	1.6	1.8	2.0
β_1	0.3078	0.3834	0.4356	0.4680	0.4872	0.5000
β_2	0.1386	0.1794	0.2094	0.2286	0.2406	0.2472
α	0.0138	0.0188	0.0226	0.0251	0.0267	0.0284

Table 3.2: Bending Values

For the case of a circular membrane, another set of equations is used to determine the maximum deflection and maximum stresses. These equations are given by [7]

$$w_{\max} = \frac{3pr^4}{16Et^3} \tag{3.5}$$

$$\sigma_{r,\max} = \frac{3pr^2}{4t^2} \tag{3.6}$$

$$\sigma_{z,\max} = \frac{3pr^2}{8t^2}(1-v) \tag{3.7}$$

In these equations for circular plates, the maximum deflection occurs at r=0, the center. The corresponding stress equations refer to radial and tangential stresses, respectively. The load, in these cases p, is the pressure load in the force of air equation. With these equations, one can then determine the output voltage when the material is subjected to a mechanical stress.

In this thesis, the membranes are approximated as thin deformable plates. the behavior of these membranes differs slightly from that of metal plates as they are extremely small and thin.

$$w_{\max} = 0.662r\left[\frac{pr}{Et}\right]^{1/3} \tag{3.8}$$

This above equation represents the maximum defection of a thin membrane under uniform pressure. This provides a reference between the actual bending of a membrane, and the use of a thin plate to substitute in a model for the membrane.

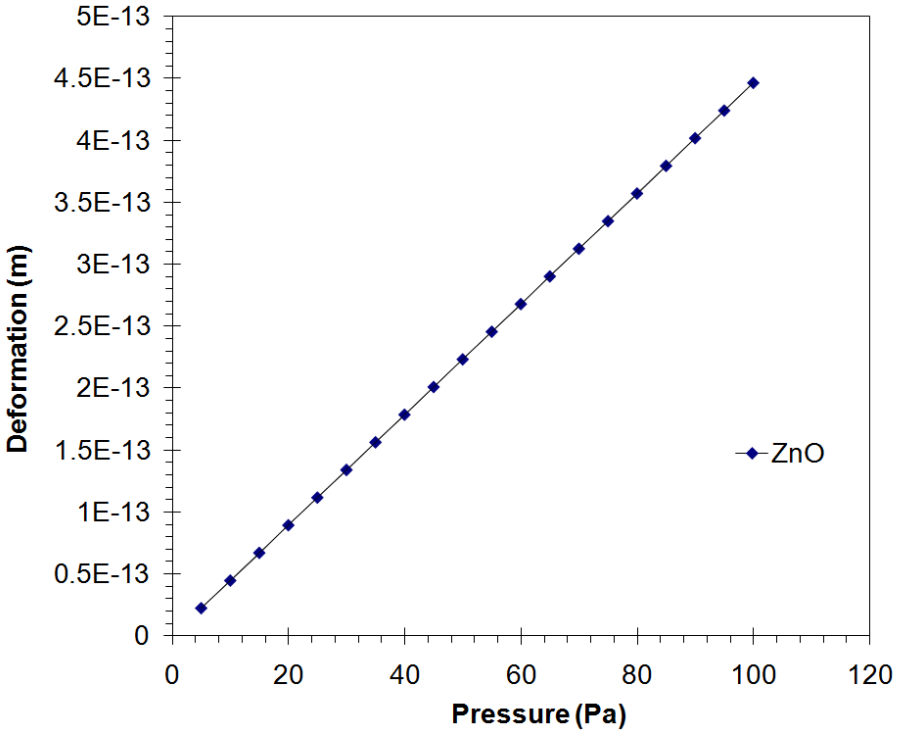

Figure 3.4: Maximum deformation for a thin plate

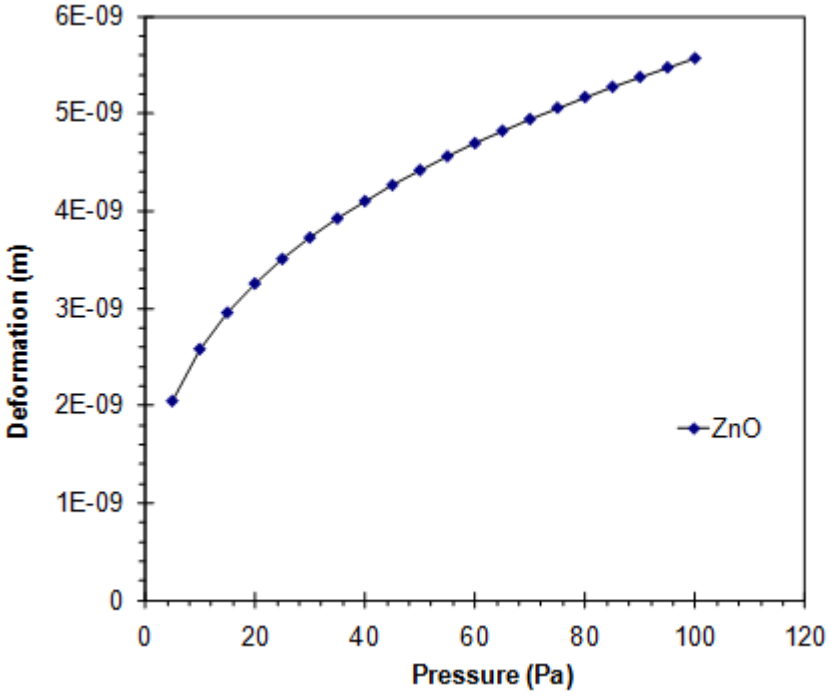

Figure 3.5: Maximum deformation for a thin membrane

Fig. 3.4 and 3.5 illustrate the use of the thin plate equation and thin membrane equation for the maximum deflection. A simulation was run for a circular plate of 5 micron radius, 0.5 micron thickness, and a Young's Modulus of 210 GPa. A steady increase in pressure was used from 5 Pa to 100 Pa over 20 iterations. The trends in graphs are different since the thin plate has a linear trend, while the thin membrane has an exponential during this simulation. This relates well with the associated equations. During the last few iterations it becomes linear. Although the thin plate results are different, they provide similar trends, from which useful analyses and application to the micro heat engine can be performed. Other past studies have also used the plate deformation equations to

approximate the membrane behavior. In the next chapter, this model of plate bending will be used to determine the output voltage of the micro heat engine, based on the deflections of the piezoelectric membrane.

Chapter 4

Formulation of the Output Voltage

In the following sections, the piezoelectric problem will be formulated in terms of output voltage, including the adaptation of the problem to the current study, and the formulation of output voltage, in conjunction with motion of the droplet in the microchannel.

4.1 Cantilever Problem

The study and application of the direct and inverse effect of piezoelectricity involves the classical problem of bending of a beam with a piezoelectric membrane. The problem of the cantilever will be examined in this section to gain insight on how deformation of the rectangular diaphragm may be adapted to it.

In the basic piezoelectric problem, a beam of unit length has a layer of piezoelectric film above it, with the appropriate contacts connecting the piezoelectric layer to a load circuit.

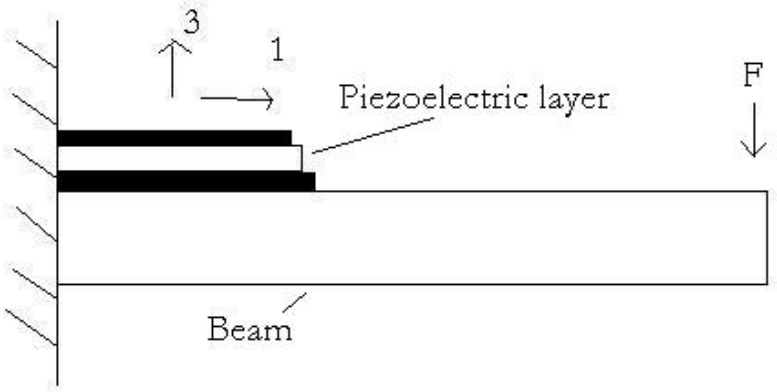

Figure 4.1: Illustration of a cantilever with piezoelectric layer

From the above figure, there is a force acting on the tip of the cantilever beam. The numbers 1 and 3 denote the axis, as defined by the governing equation for piezoelectricity. The first step to determining the output voltage from the applied force is to find the maximum stress acting along axis 1. This is given by

$$\sigma_{1,\max} = \frac{Flt_{beam}}{2I_{beam}} \tag{4.1}$$

From Eq. (1.2), the output electric displacement in axis 3 is given by

$$D_3 = d_{31}\sigma_{1,\max} \tag{4.2}$$

The voltage can then be found by

$$V = E_3 t_{piezo} = \frac{D_3 t_{piezo}}{\varepsilon} = \frac{F l t_{beam} t_{piezo}}{2 \varepsilon I_{beam}} \tag{4.3}$$

This indicates that we need to know the direction of polarization and the direction of the maximum stress. Since both of these are known for the rectangular membrane, we can proceed to combine them to develop a model for the output voltage of the micro heat engine.

4.2 Square Membrane Output

The cantilever approach has limited applicability to the current configuration. Additional configurations of the micro heat engine is to add piezoelectric membranes to both ends of the channel, or by adding them to the top, bottom, or side of a microchannel, similarly to past work of Whalen et al. [36]. By adding a rectangular microchannel to the top or bottom of the microchannel, one can take advantage of the size, as opposed to the ends. For a circular microchannel with a diameter of 1 μm, it is more difficult to fabricate and attach a membrane, as compared to a rectangle of 2 μm by 2 mm. In this way, one can take advantage of the length of the microchannel to attach membranes and associated electric circuitry.

To find the voltage output of the configuration, the formulations in sections 3.3, and 4.1 will be combined. By using Eq. (1.2), we can find the electrical polarization as a function of the piezoelectric constant of the material, stress, permittivity, and electrical field. Since the last two are not present in the current case, we are left with the piezoelectric constant and the applied stress. In section 3.3, a model was formulated for the deformation of a rectangular or square plate and membrane. With this model, it is possible to find the output voltage for a square membrane.

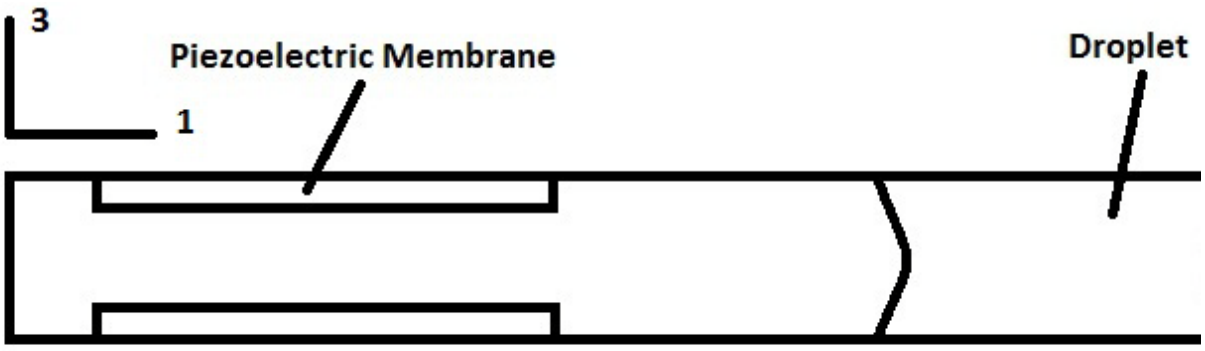

Figure 4.2: View of axis of the micro heat engine

Fig. 4.2 shows a close-up view of one side of the micro heat engine. In this view, the axis is labeled for the piezoelectric membrane. In this problem, assume that polarization of the piezoelectric material is poled in the z direction, or the direction of axis 3, which is common in most piezoelectric elements. It is also assumed that the electrodes attached to the piezoelectric membrane are parallel. For example, the electrodes are attached on the bottom and top of the membrane,

instead of the side of the membrane, on the outside of the channel. This is commonly found when using a piezoelectric membrane in this manner.

If the contacts are stacked, From Eq. (1.2), the electrical polarization can be found as a function of the piezoelectric constant and applied stress. Combining this with the formulation in section 3.3,

$$D_3 = dT_3 \tag{4.4}$$

When the prior models are substituted into this equation,

$$D_3 = d_{31}\frac{\beta_2 p b^2}{t^2} \tag{4.5}$$

In this case, p is equal to the pressure applied by air in the chamber.

$$D_3 = (d_{31})\left(\frac{\beta_2 b^2}{t^2}\right)\left(\frac{RmT}{V}\right) \tag{4.6}$$

To find the resultant output voltage, Eq. (4.6) can be substituted into Eq. (4.3), by the following relation,

$$\frac{D}{\varepsilon} = E \tag{4.7}$$

$$Et = V \tag{4.8}$$

The electric field is reduced to zero but in this case is used to show that the output voltage can be related to the electric potential and dielectric constant. This leads to the following result,

$$V = \left(\frac{d_{31}\beta_2 b^2}{t_{Piezo}\varepsilon} \right) \left(\frac{RmT}{V} \right) \tag{4.9}$$

Eq. (4.9) is multiplied by 2 because it refers to a situation where force creates a stress in a single direction, leading to Eq. (4.8). The deformation of a membrane creates stress in two directions, both axes 1 and 2.

$$V = 2\left(\frac{d_{31}\beta_2 b^2}{t_{Piezo}\varepsilon} \right) \left(\frac{RmT}{V} \right) \tag{4.10}$$

In the case of coplanar electrodes, the above equations differ slightly. Recall that the stress matrix considers a normal stress and shear stress along each axis. With coplanar electrodes, the shear stress is taken into consideration because of the polarization in axis 1. To find the output voltage in this situation, it can be shown that

$$E_1 = \frac{D_1}{\varepsilon} \tag{4.11}$$

$$V_1 = E_1 l \tag{4.12}$$

$$D_1 = d_{15} T_5 \tag{4.13}$$

Using the above equations, and rearranging to find the output voltage, it can be shown that

$$V_1 = \frac{d_{15} T_5 l}{\varepsilon} \tag{4.14}$$

Eq. (4.14) shows how a difference in electrode placement for the membrane may result in a different output voltage.

4.3 Circular Membrane Output

Similarly, a circular membrane can be implemented if this shape is desired. This can be placed in similar areas as the rectangular membranes. It can also be placed at either end of the channel, although there may be a difference in fabrication difficulty when placing it in smaller areas. When formulating a model for the output of a circular membrane, the equations for a rectangular membrane can be combined with a circular membrane modeling, while removing the portion of the equation that refers to the rectangular membrane.

$$V = 2\left(\frac{d_{31}}{\varepsilon}\right)\left(\frac{RmT}{V}\right)_R\left(\frac{\beta_2 b^2}{t_{Piezo}}\right) \tag{4.15}$$

Equation (4.15) has been separated so it is clear which terms are removed and replaced with the circular membrane relations.

$$V = \left(\frac{d_{31}}{\varepsilon}\right)\left(\frac{RmT}{V}\right)_R \frac{3r^2}{8t^2}(1-v) \tag{4.16}$$

The above equation utilizes the maximum stress for a circular membrane in the z direction, Fig. 4.2, keeping the relation for the electric field and pressure terms. This is valid for circular membranes where the electrodes are parallel. For the situation where electrodes are coplanar, the stress term is changed slightly to reflect this, as well as the general solution for voltage.

$$V_1 = \frac{d_{15}l}{\varepsilon}\left(\frac{RmT}{V}\right)_R \frac{3r^2}{4t^2} \tag{4.17}$$

Equation (4.17) represents the solution for a circular piezoelectric membrane under uniform pressure.

This completes the model for the output voltage of a rectangular piezoelectric membrane on a square membrane subjected to fluid motion. In the next chapter, validation and predicted results will be presented for the model formulated in this chapter. Results of the simulations will be presented and discussed for several test cases.

Chapter 5

Results and Discussion

In chapters 1-4, a new micro heat engine was described and models were developed to predict the movement and behavior of the droplet and system. Various properties and characteristics of the system were also discussed. This chapter presents a validation for the model, as well as results of a simulation based on the models and equations formulated. The results will provide a comparison between the square channel and the cylindrical channel with circular cross-section, as well as varying properties of the system.

5.1 Validation of the Piezoelectric Model

Once the theoretical models have been completed, one must validate the formulations before further discussion about results. The validation will be conducted in this section, by validating each sequence of the model.

5.1.1 Bending of a Rectangular Membrane

To validate the bending of the membrane, a similar process will be completed by treating the membrane as a simply supported rectangular membrane of dimensions a x b. For the bending of the rectangular membrane, consider a Fourier series with the following boundary conditions:

$$\begin{aligned} \frac{\partial^2 w}{\partial x^2} &= 0, \qquad at\ x = 0\ and\ x = a \\ \frac{\partial^2 w}{\partial y^2} &= 0, \qquad at\ y = 0\ and\ y = b \end{aligned} \tag{5.1}$$

According to Ref. [38], the deflection of the membrane at an arbitrary point can be expressed as

$$w(x,y)=\frac{a^4}{D\pi}\sum_{m=1}^{\infty}\sum_{n=1}^{\infty}\frac{q_{mn}}{\left(m^2+n^2\left(a^2/b^2\right)\right)^2}\sin\left(\frac{m\pi x}{a}\right)\sin\left(\frac{n\pi y}{b}\right) \tag{5.2}$$

D in this case represents the rigidity of the plate. The rigidity of the plate is dependent on the material and it is a function of the thickness, Young's modulus, and the Poisson's ratio in the following equation,

$$D=\frac{Et^3}{12\left(1-v^2\right)} \tag{5.3}$$

The maximum deflection of the plate can be found at the centre due to symmetry. It can be found by first calculating the uniform load q_o. This is found with the following equation,

$$q_{mn}=\frac{4}{a^2}\int_0^a\int_0^b q(x,y)\sin\left(\frac{m\pi x}{a}\right)\sin\left(\frac{n\pi y}{b}\right)dxdy=\frac{4q_o}{a^2}\frac{a^2}{mn\pi^2}\cos\frac{m\pi x}{a}\Big|_0^a\cos\frac{n\pi y}{b}\Big|_0^b \tag{5.4}$$

The maximum deflection can then be substituted into Eq. (5.2) to obtain

$$w(x,y)=0.244\frac{16q_oa^4}{D\pi^6} \tag{5.5}$$

There are now two methods by which one can determine the maximum deflection. Eq. (3.2) will be called method 1 and Eq. (5.5) will be called method 2. By modeling the membrane of the piezoelectric material with both methods, they may be compared against each other to validate. By examining the two equations it can be seen that method 1 does not contain rigidity in its formula whereas method 2 does. Instead it uses a simplified version where the modulus of elasticity is used.

The two methods have also been carried out in different manners, method 2 employing the use of a Fourier series. Table 5.1 outlines the constants used for this example, using ZnO as the piezoelectric material.

Young's modulus (E)	Thickness (t)	Poisson's ratio (v)	A	B	Alpha
210 GPa	0.5 microns	0.3	8 microns	5 microns	0.0237

Table 5.1: Constants used for simulation

A uniform pressure of 5kPa was applied to the rectangular membrane with an increase of 5kPa over 20 iterations. Fig. 5.1 is the result of simulating both methods under the same conditions. In order to validate the use of Eq. (3.2) in the micro heat engine model, the results from the simulation must compare positively. The trends initially start off from the same point, but then increase differently. This may be due to their main difference, Eq. (5.4) contains the term for the rigidity of the material whereas Eq. (3.2) does not include this factor. According to Ref. [47], the form of Eq. (3.2) can also be found as

$$w_{\max} = \frac{\alpha p b^4}{D} \tag{5.6}$$

The term D which incorporates the Poisson's ratio of the material has been simplified to Et^4. By substituting Eq. (5.6), a more realistic result is obtained.

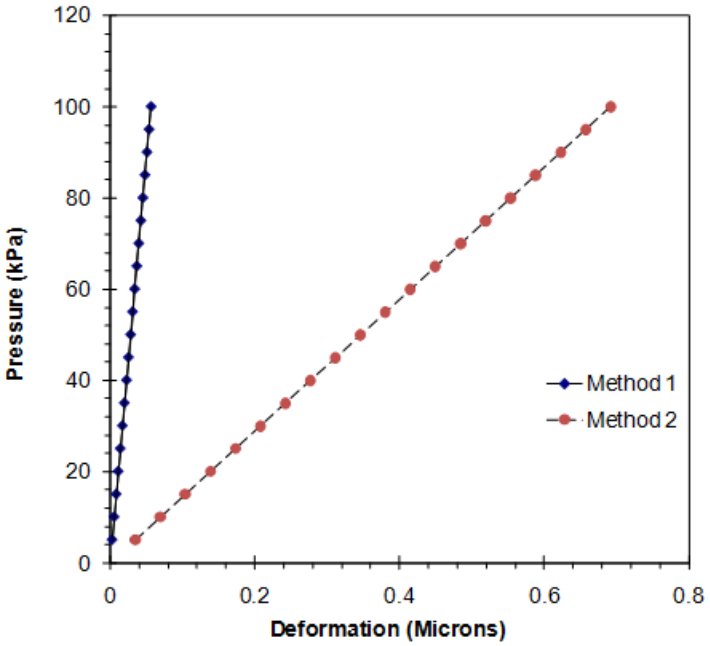

Figure 5.1: Validation of the deformation of the membrane

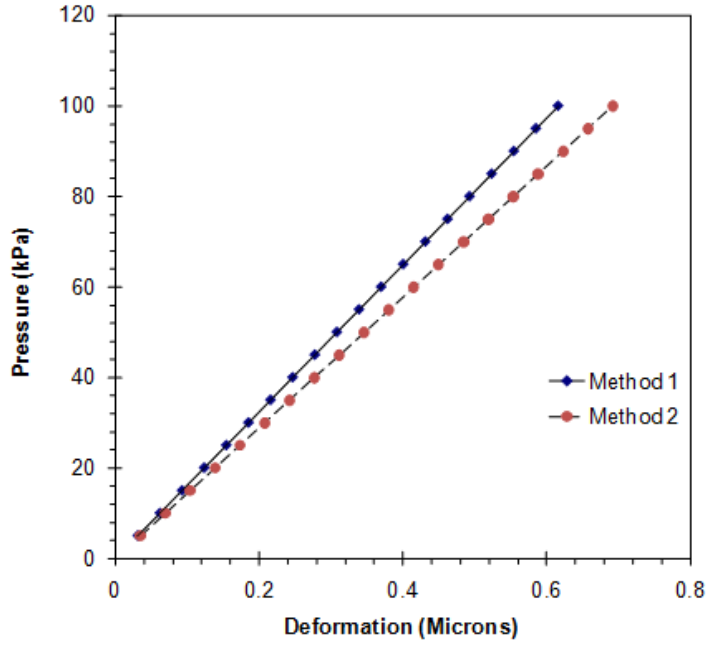

Figure 5.2: Validation after incorporating Poisson's ratio into the equation

From Fig 5.2, after the addition of Poisson's ratio, the results are quite similar when finding the deflection of a rectangular plate. The two curves separate slightly as they reach higher deflections, but are still relatively close. These results provide useful verification of the models developed in chapters 2 and 3.

5.1.2 Piezoelectric Effect

Due to the unique piezoelectric mechanism in the present microchannel heat engine, it is difficult to precisely validate the relationship between the bending of the rectangular membrane in relation to the piezoelectric effect. At this point in time an experimental setup has not been completed and therefore it is not possible to measure the amount of piezoelectric effect generated. As a result, the model will be compared against another previous study of similar nature. The model will be compared against the experimental values obtained from the design and testing of a prototype P^3 engine [37]. Although not exactly the same configuration, the design uses a similar mechanism and principles of the piezoelectric effect and working fluid as the current design in this thesis. Fig. 5.3 illustrates the cycle for the P^3 engine.

The P^3 engine consists of a cavity enclosed by two membranes, a piezoelectric membrane and a heater. Inside the cavity, there is a vapor which acts as the working fluid for the system. Heat is added via the heater membrane on the

bottom. When heat is added, the vapor increases in temperature and pressure. This increase of pressure causes the piezoelectric membrane to flex similar to the process in the current micro heat engine. In comparison to the micro heat engine in this thesis, the vapor in the P^3 engine works like the air, as it is being compressed by the droplet as it moves down the channel. As the compression of air causes the membrane to flex in the micro heat engine, so does the vapor cause the membrane to flex outwards. The specific gas constant for water vapor is almost twice the value for dry air. This however does not affect the relationship between the pressure and deflection of the membrane, only the relationship between the pressure with respect to time.

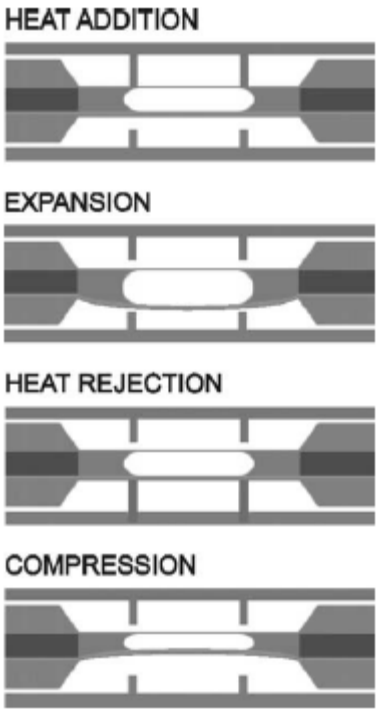

Figure 5.3: P^3 engine illustration of cycle

The processes for translation of pressure to voltage generation in the piezoelectric membrane are similar. Values and trends from this engine should be similar to values obtained by adapting the model from this thesis to the specifications of their engine. Design of the complete P^3 engine is not necessary since the focus here is the conversion of deformation to voltage in the membrane. Thus, we need only to evaluate the dimensions of the piezoelectric membrane, piezoelectric material and approximately the increase of pressure. Using these initial conditions in the present model should yield similar results. For example, given the constants and geometries of the membrane, for a deformation x of the membrane, it yield a voltage V based on a pressure p which can be compared to calculations in this thesis.

Young's Modulus	130 GPa
Length	3mm
Width	3mm
Thickness	2.4 microns
Dielectric Constant	1300
Beta	0.1386
Alpha	0.0251

Table 5.2: Constants and parameters used to validate against P^3 engine

Table 5.2 shows the constants and parameters used to simulate the P^3 engine. The geometries of the P^3 engine have been taken from Ref. [37], as well as constants for the material.

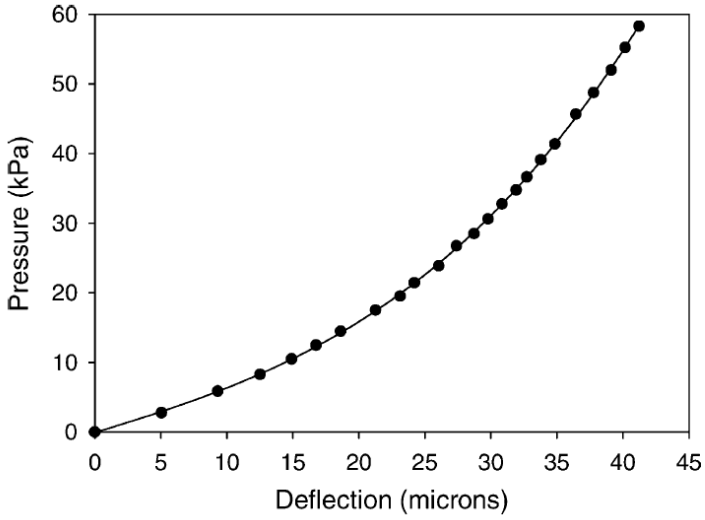

(a)

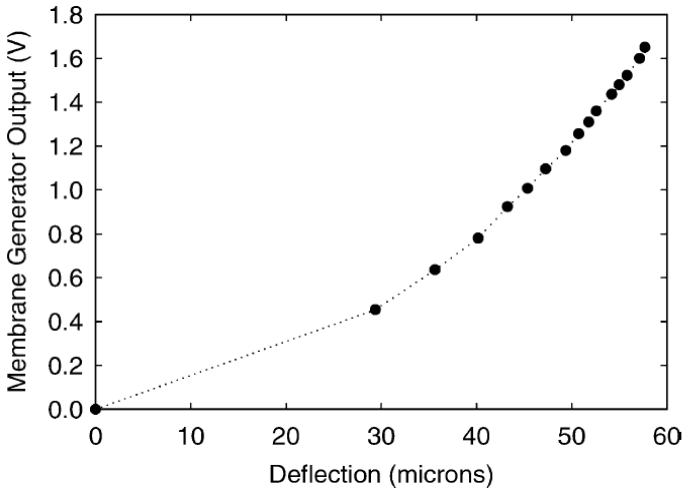

(b)

Figure 5.4: (a) and (b) show experimental results of the P^3 engine

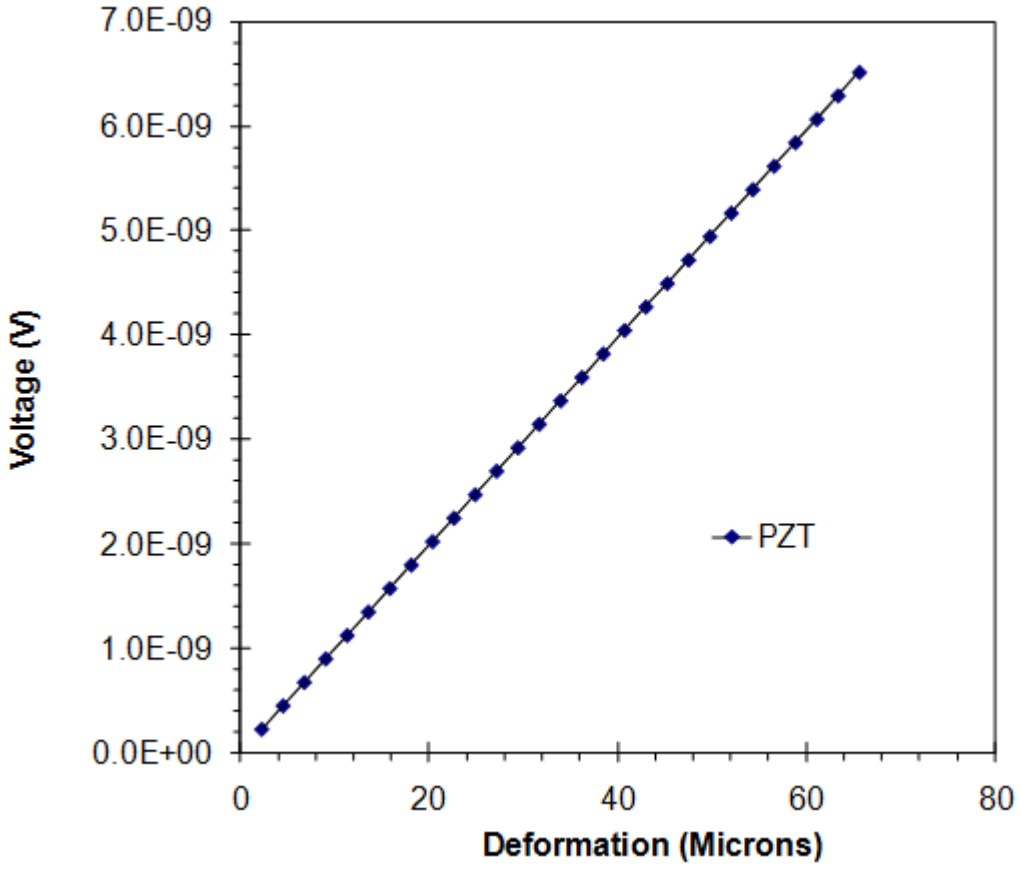

Figure 5.5: Results of PZT for P^3 engine specifications

In Fig. 5.5, the deformation vs. voltage follows a linear increase, unlike the experimental values. According to the experimental values for the P^3 engine, a 30 micron deformation of the piezoelectric membrane results in an open circuit voltage of about 0.4V.

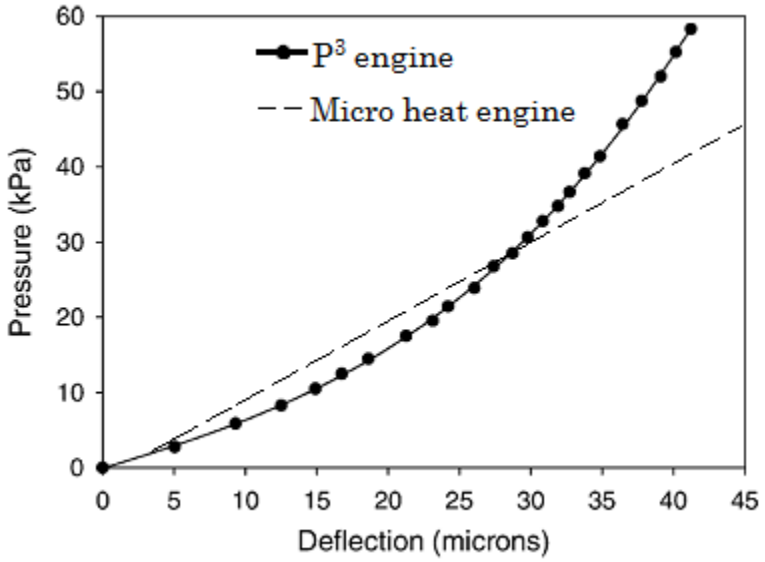

Figure 5.6: Micro heat engine values plotted against P^3 experimental values

The initial deformation of the membrane will be compared against the present model. Fig. 5.6 shows the predictions of membrane deformation, with a linear increasing trend, differing from the experimental values. However, the predicted and measured values for deflection are in close range at low pressures. For example, a 30 kPa pressure on the membrane produces approximately a deformation of 30 microns in both cases and at 20 kPa the P^3 engine deflects 25 microns and the micro heat engine deflects 22 microns. At pressures above 30 kPa, values in both cases vary greatly. There may be a difference in the conditions or constants for the output voltage used since the specific PZT was not documented by the authors. However, the close agreement, relative distance between deflection points, between results nevertheless provides useful validation of the model for certain points.

The cantilever is a common problem presented in textbooks. An attempt will now be made to validate the model by comparing it to a sample problem found in Ref. [7]. The example consists of a cantilever beam with a piezoelectric layer bonded on top, with a portion of the length of the beam. The piezoelectric layer is located between two electrodes. A force acts on the tip of the beam to displace it. The associated figure is Fig. 4.1 and the associated equations are (4.1) to (4.3). Initially they show that the force creates a longitudinal tensile stress and a shear stress. The shear stress is neglected because the direction of poling is in the direction of the third axis. An equation for the maximum stress is formulated for the beam in Eq. (4.1). Similarly, there exists a maximum stress in the membrane in Eq. (3.4). The general constitutive equation and a solution for the electrical polarization follow from Eq. (4.2). It was determined that the electrical polarization can be found by multiplying the piezoelectric constant and the maximum stress in axis 3 of Eq. (4.4). This relates the output voltage, V, in equation 4.3 to the end result, which is the same as found in Eq. (4.7) and (4.8). These relations can be used, as there is no electrical field present in the general equation, thus the second term in the equation of the electrical field reduces to zero. Thus, it can be verified that the method is valid and the deviation is minor, which provides additional useful validation of the model.

5.1.3 Fluid Flow in a Circular Microchannel

This section aims to validate the model used for fluid flow in the microchannel with a circular shape. Recall that the fluid flow in the system uses a slug flow approximation. It involves three forces: thermocapillary, air, and frictional forces. The force of air in the microchannel was found to be the difference between the pressures in both sides of the air cavity within the microchannel, multiplied by the area.

The equations for the thermocapillary force and force of air can be validated as they are not specifically related to the shape of the channel. From Eq. (2.7), the thermocapillary force is a function of the differences in capillary pressure between the left and right insides of the droplet and the geometry of the channel. This equation is suitable for a rectangular or circular membrane, because the variables are interchangeable with rectangular and circular shapes. The shape factor's value changes with respect to the shape of the channel. The height of the microchannel and the cross-sectional area also change accordingly, without modifying the governing equation.

The force of air and thermocapillary force are the same for both types of channels, but not the frictional force. Eq. (2.8) represents the solution for the

frictional force in a rectangular microchannel. The model for the fluid flow can be found in Eq. (2.13)

With the slug flow approximation, the model was used to determine the droplet displacement, force of friction, force of air, thermocapillary force, and pressure with respect to time, among others. With these values, parameters were also modified to determine the effects of certain variables on the droplet displacement. It is the objective of this section to validate the model in Eq. (2.13) by comparing against the simulation completed by Glockner [48]. The validation will be based on thermocapillary pumping inside microchannels of similar dimensions with the working fluid and gas as water and dry air respectively. This will compare graphs of a similar nature for a rectangular membrane and a circular membrane. Due to the similarities of the slug flow approximations, the trends should be similar.

Channel height	1 micron
Channel length	2000 microns
Channel depth	100 microns
Density of air	1.1624 kg/m^3
Density of water	998 kg/m^3

Table 5.3: Initial parameters used to compare against Glockner's data [48]

Table 5.3 displays the initial parameters and substance properties used in previous studies. According to Glockner's work [48], each side of the droplet was maintained at either a high or low temperature. Initial temperatures for this comparison are 20 ^{o}C and 30 ^{o}C, with one side increasing gradually. Upon initial inspection of results from this situation, Fig 5.7, the predictions agree well with the results reported in [48]. During early stages of droplet motion in the microchannel, there is a relatively large displacement at the start of the cycle, due to a large increase in bulk velocity. Fig. 5.6 illustrates the cylindrical channel with circular cross-section results for the droplet bulk velocity, as well as data obtained previously by Glockner [48] for a rectangular microchannel. Although different values are obtained due to different configurations, the trends are similar in shape.

Near the origin of Fig. 5.7, there is a significant jump in the droplet's bulk velocity, while in Glockner's data, there is a jump in bulk velocity, followed by a smoother transition at each time step. The large step change in bulk velocity may be due to how the temperature was incremented in each case. In the case of Glockner's study, the temperature curve is relatively smooth and almost linear. In the case of the circular membrane, the temperature curve was not used. The values were obtained from Matlab. Instead, the left and right temperatures of the droplet were specified. Although there is a difference in values for each trend, the importance is that the shapes of the trends are similar. The values are expected to be different because the channels themselves are different. The contact area between the droplet and the channel wall is smaller in the circular channel as

opposed to the rectangular channel due to the shape. This reduction in interface reduces the frictional force opposing the droplet motion. Glockner's results show approximately a bulk velocity of 1,800 microns/s, while the model for a circular microchannel has a maximum bulk droplet velocity of about 2,400 microns/s. The results for TCP are for half of the cycle, in the portion where the droplet proceeds with a positive displacement. It stops at about the time when the forces balance, after which the droplet moves backwards.

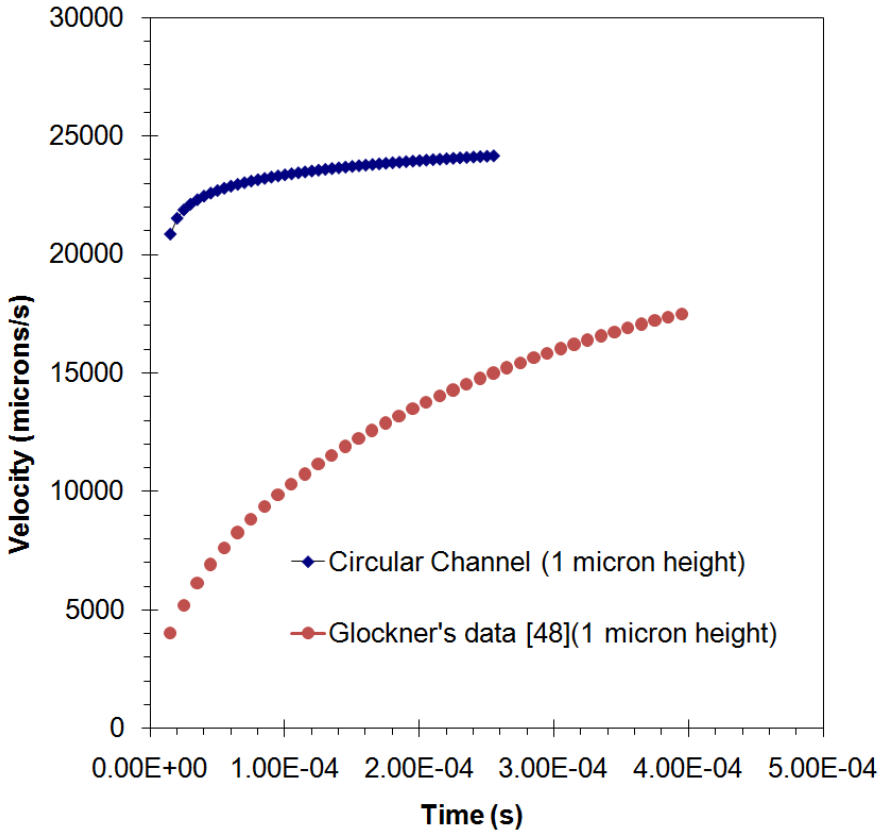

Figure 5.7: Bulk velocity in the microchannel

The graphs do not behave exactly the same, due to the different geometrical configurations. With a large bulk droplet velocity in the cylindrical

channel with circular cross-section, it is expected that the droplet will displace much faster than a rectangular channel with the same droplet mass.

5.2 Output Voltage in the Micro Heat Engine

Output voltage from the micro heat engine can be obtained based on the model that has been formulated in prior chapters. As discussed earlier in the thesis, there can be many variations of the placement of the piezoelectric membranes and their number. A variation to produce a higher open circuit voltage would be placement of four membranes on each opposing end. This would result in the membranes placed on each longitudinal side, acting oppositely when each cycle completes. As the droplet moves forward, the four membranes on side A would experience a stress resulting in an electric field. As the droplet moves back, membranes in side B would experience the same effect.

To determine the effects of the piezoelectric membranes on thermocapillary pumping, a single membrane in a channel will be examined. Table 5.4 shows the constants and parameters used in simulation to analyze the potential of the micro heat engine. In all cases, one side of the channel remains at a constant temperature, while the opposing side has an increase in temperature. One complete

cycle will be studied for the effects on the output voltage. The piezoelectric material, ZnO, has been chosen due to its full availability of property data. ZnO is not commonly used for sensing, due to its low coupling factor. The dielectric constant for ZnO is 8.5, one of the lowest dielectric constants of commonly used piezoelectric materials. It is commonly used for actuation.

Channel height	1 micron
Channel length	2000 microns
Channel depth	100 microns
Density of air	1.1624 kg/m^3
Membrane thickness	0.5 microns
Membrane length	150 microns
Membrane width	100 microns
Alpha	0.0138
Dielectric constant	8.5
Coupling factor	0.075
Young's modulus	210 GPa
Density of water	998 kg/m^3

Table 5.4: Parameters and constants used for 0.5 micron thick ZnO membrane

Based on models developed in chapter 4 and results in Fig. 5.9, the voltage vs. deformation follows a linear trend. The graph follows a linear increase and reverses back upon itself, as the heater is turned off and the droplet in the

microchannel starts to move back to its original position. This can be explained due to the linear relationship between the pressure and deformation. The low voltage can be explained by the poor coupling factor k, which is the material's ability to convert mechanical stress into electrical energy.

The low deformation can be attributed to the low pressure in the microchannel. In other cases in this thesis, the pressures were in the kPa range, while the pressure here inside the microchannel is in the Pa range. Fig. 5.10 shows the deformation with time for the ZnO membrane.

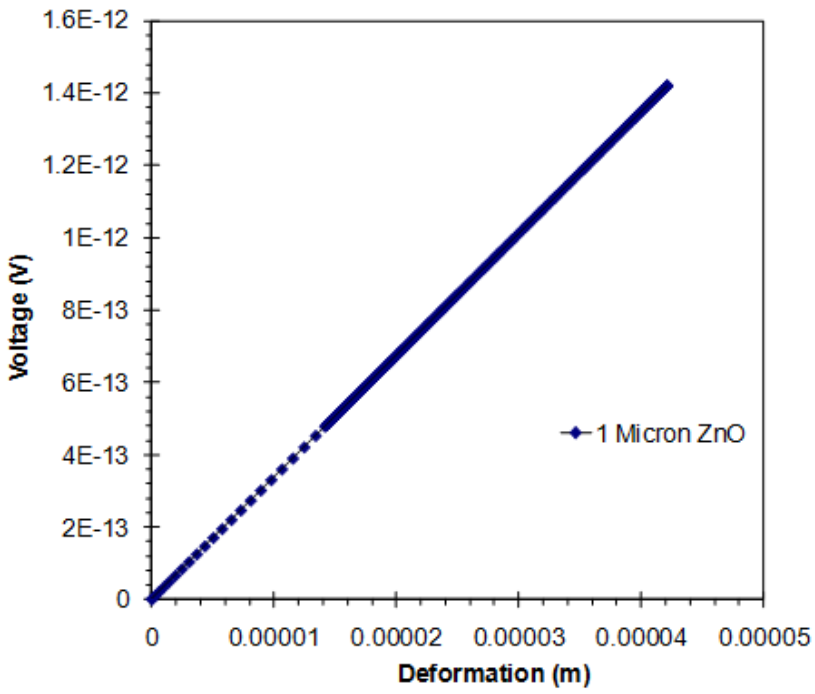

Figure 5.8: Simulated results of voltage and deformation for ZnO membrane

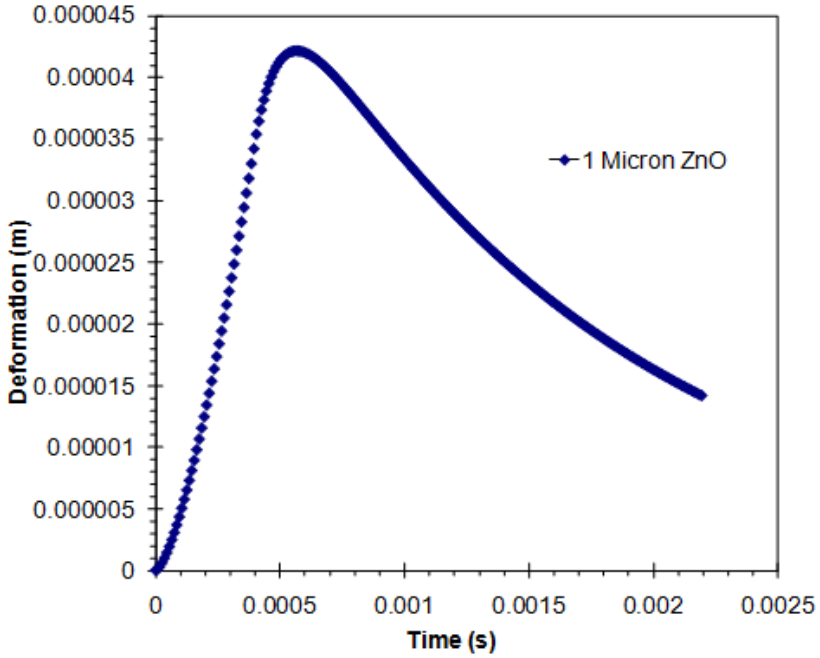

Figure 5.9: Deformation of a ZnO membrane (1 micron)

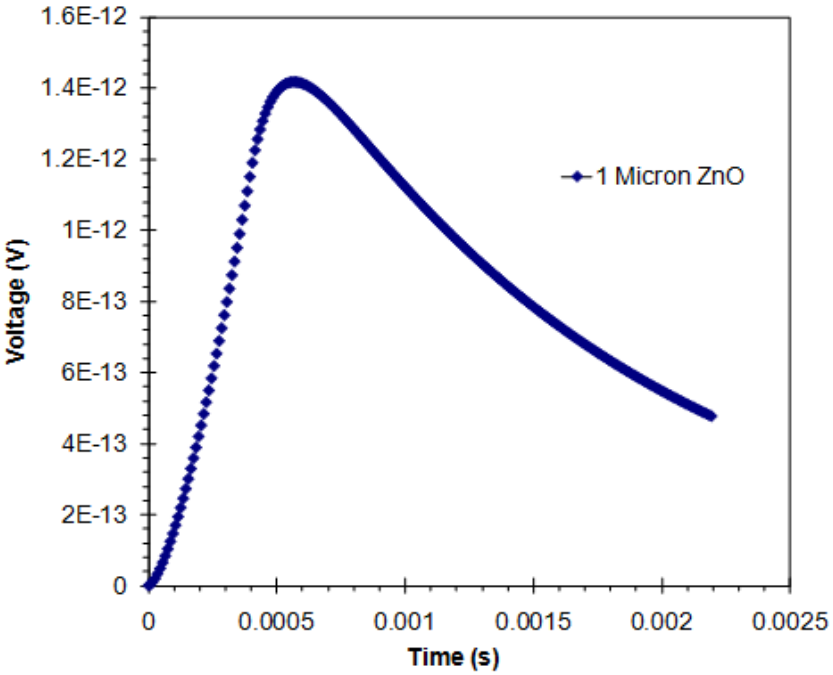

Figure 5.10: Output voltage of the ZnO membrane (1 micron) under mechanical stress

The curve in Fig. 5.10 follows the same trend as the displacement of the droplet. This occurs because they are directly proportional to each other. In this case, a maximum deformation occurs quickly in relation to the amount of time for the cycle to complete. The maximum deformation occurs when the droplet has a maximum displacement along the x axis, which causes the pressure to accumulate in this side of the channel. This causes the membrane to flex. A maximum deformation of the membrane is about 0.02 microns for a pressure of about 400 Pa. Since the graphs for the deformation and voltage follow linear trends, the open circuit voltage for the membrane is directly proportional to the displacement of the droplet, and the deformation of the membrane. From Fig. 5.11, as the droplet reaches its maximum displacement along the microchannel, the piezoelectric membrane has a maximum output voltage of 1.4 pV.

Fig. 5.12 shows a comparison of the voltage against forces. Figures 5.12 (a), (b) and (c) all contain a single line which describes the force fluctuation as the voltage changes. As the heat is applied, there is an increase in the thermocapillary force in the positive direction. When examining the frictional force, the curve originates at the origin and proceeds left. As the droplet starts to move, there is an increase in the frictional force in the negative direction. It is interesting to note that the voltage continues to increase in both cases, after the force of air and thermocapillary force have reached their maximum values, and then start to decrease. This may be explained by the net force on the droplet. These maximum

values occur before the droplet has reached the maximum displacement, at separate times. The thermocapillary force occurs close to the maximum bulk velocity of the droplet. The maximum force of air occurs when the droplet has reached its maximum displacement, to oppose the acting thermocapillary force.

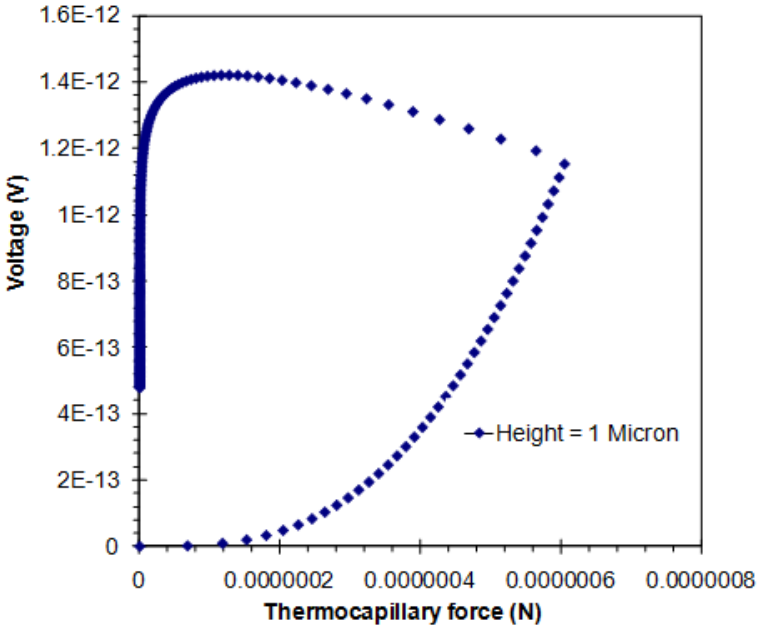

(a)

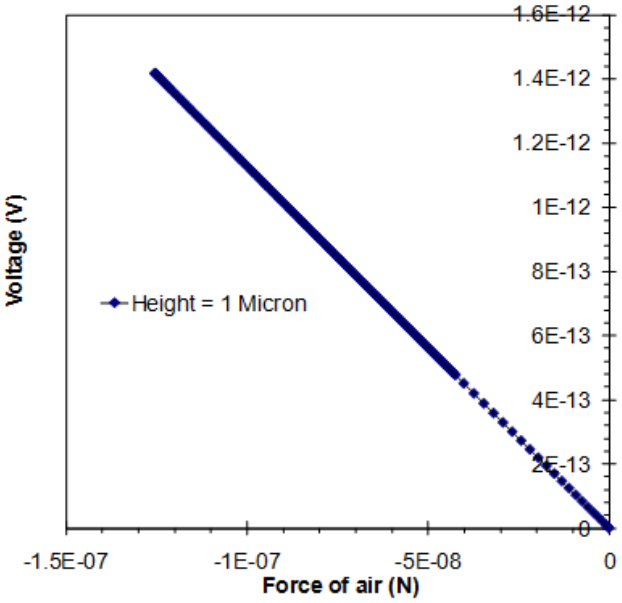

(b)

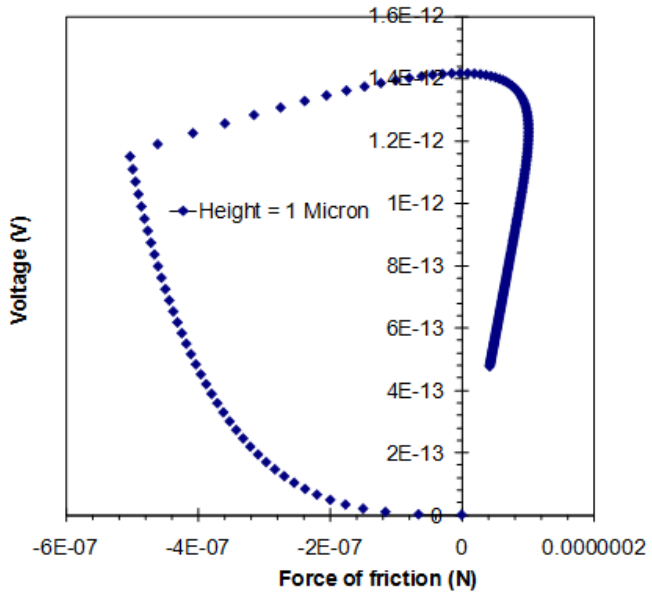

(c)

Figure 5.11: Force and voltage comparison for (a) thermocapillary, (b) air and (c) friction forces

5.3 Output Voltage at Varying System Parameters

The model developed in previous chapters was further applied to sensitivity studies of the system. In order to understand the most significant parameters in terms of voltage output of the system, various dimensions and properties were examined and modified.

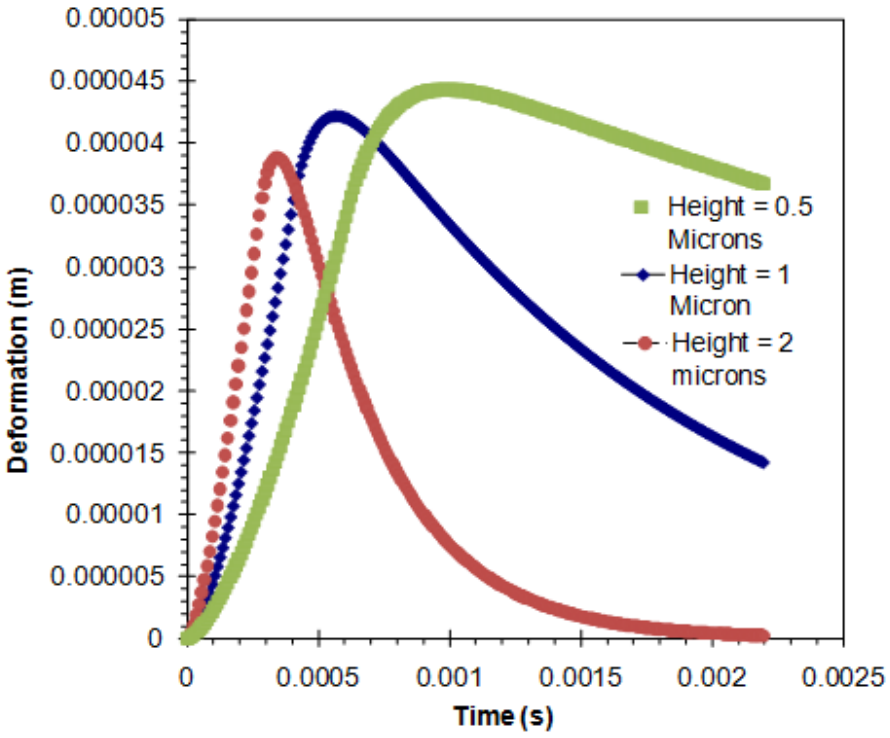

Figure 5.12: Membrane deformation at varying heights

The geometry of the microchannel and material properties were changed. There are three varying heights: 0.5 microns, 1 micron, and 2 microns. As well as

changing the height, a change in the material of the piezoelectric membrane was also examined. The difference between common materials ZnO and PZT was investigated.

Fig. 5.13 shows the effect of varying channel height on the deformation of the membrane. It can be seen that a smaller microchannel results in larger deformations of the membrane. There is an increase of deformation with decreased channel height. Also, there is a prolonged duration of membrane return. Although there may be a beneficial increase in the deformation, a smaller microchannel results in a membrane that takes longer to return to its initial position at zero deflection. This implies an increase in cycle time. For a system that produces electricity, more power cycles are desired in shorter amounts of time. Thus, it is beneficial for the microchannel to be larger in size, although there is an increase in deformation, and as a result, an increase in output voltage. The increase in deformation is small in relation to the increase of time for the system to complete one cycle.

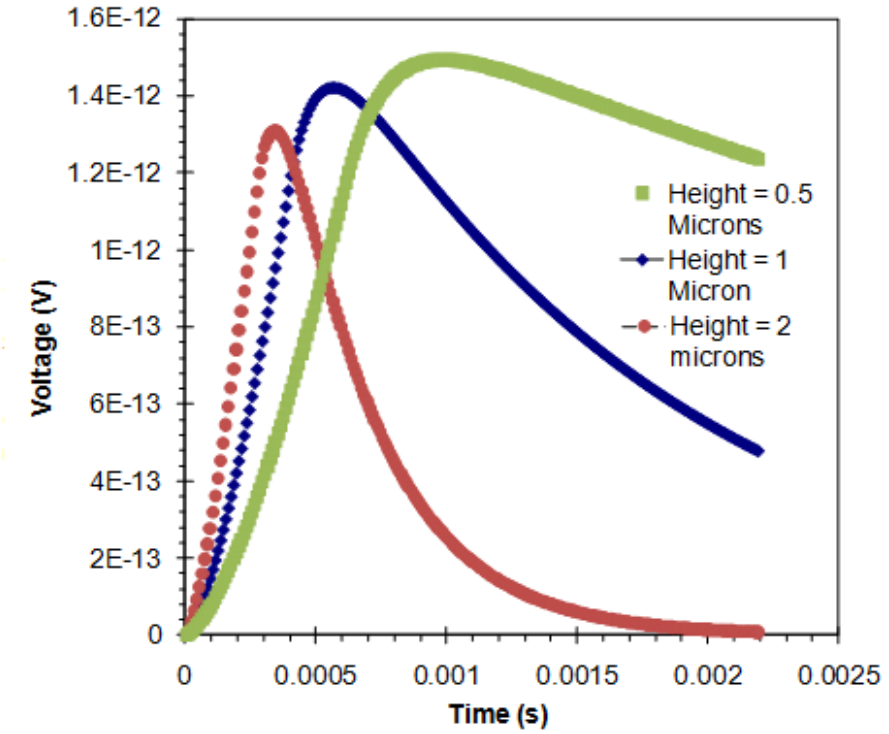

Figure 5.13: Voltage differences at varying heights

This difference in membrane deformation contributes to the difference of voltage output for each of the varying heights of the microchannel. Fig. 5.14 displays the difference in voltage between these heights. It can be observed, like the deformation, that the smaller channel yields a larger deformation. This occurs because of the pressure acting on a much smaller area. Compared against each other, the difference in voltage is not large. The droplet takes longer to return to its original position in the channel with a smaller height, and thus takes longer to complete a cycle and start a new cycle. In the time it takes the 0.5 micron channel to complete one cycle, the 2 micron height channel can complete two cycles and

effectively generate twice the voltage, more than making up for the difference in maximum voltage.

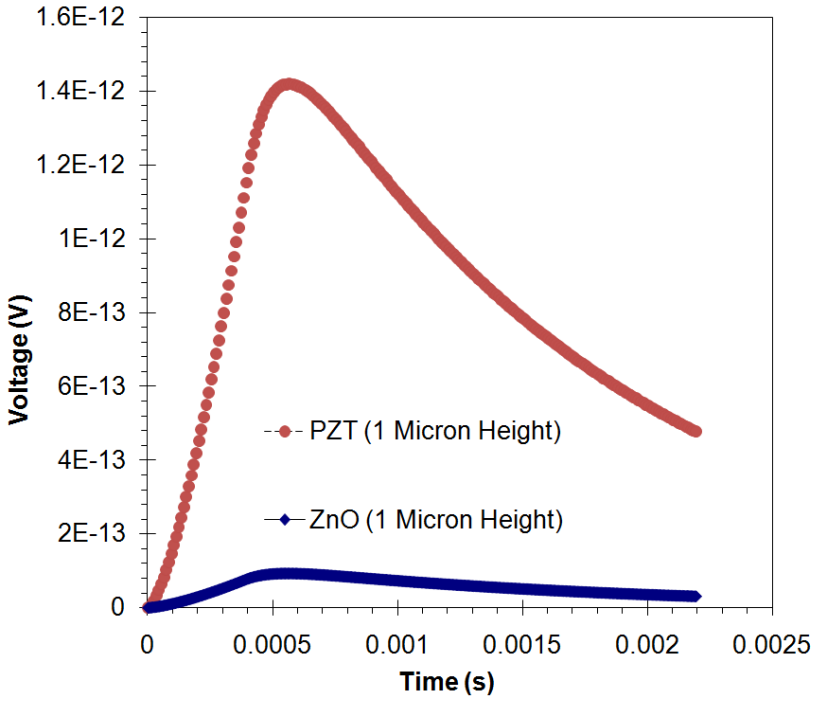

Figure 5.14: Material comparison and effects on output voltage

An important aspect of the design is the piezoelectric membrane and material used. The material depends on the function of the device. For sensing applications, materials with high voltage outputs are desired. For actuators, low dielectric constants are sought after. For this particular operation, the material best suited would also be one that provides the highest output voltage. High coupling factors are most desirable. Fig. 5.15 illustrates voltage output values for two types of materials, ZnO and PZT. Both are commonly used, but for different applications. PZT is found to have a higher output voltage than ZnO. This is a result of the

properties associated with the material. The coupling factor, k, varies greatly between the two materials compared. PZT has a coupling factor of 0.6 while ZnO has a coupling factor of 0.075. Recall that the coupling factor is the materials ability to convert one form of energy to another. This explains the large difference in output voltages between the two materials.

Another aspect that can be changed is the geometry of the membrane which will have an effect on the output voltage of the system. Fig. 5.16 illustrates the effects of the change in thickness of the membrane. The 0.5 micron membrane is more effective with a larger output voltage than the thicker membranes. This is apparent since a thicker membrane reduces the ability to deform it. Thus, geometries of a membrane that support deformation are more useful in generating more voltage output. A membrane with a larger force area would be suitable, but would also require the width of the channel to be increased.

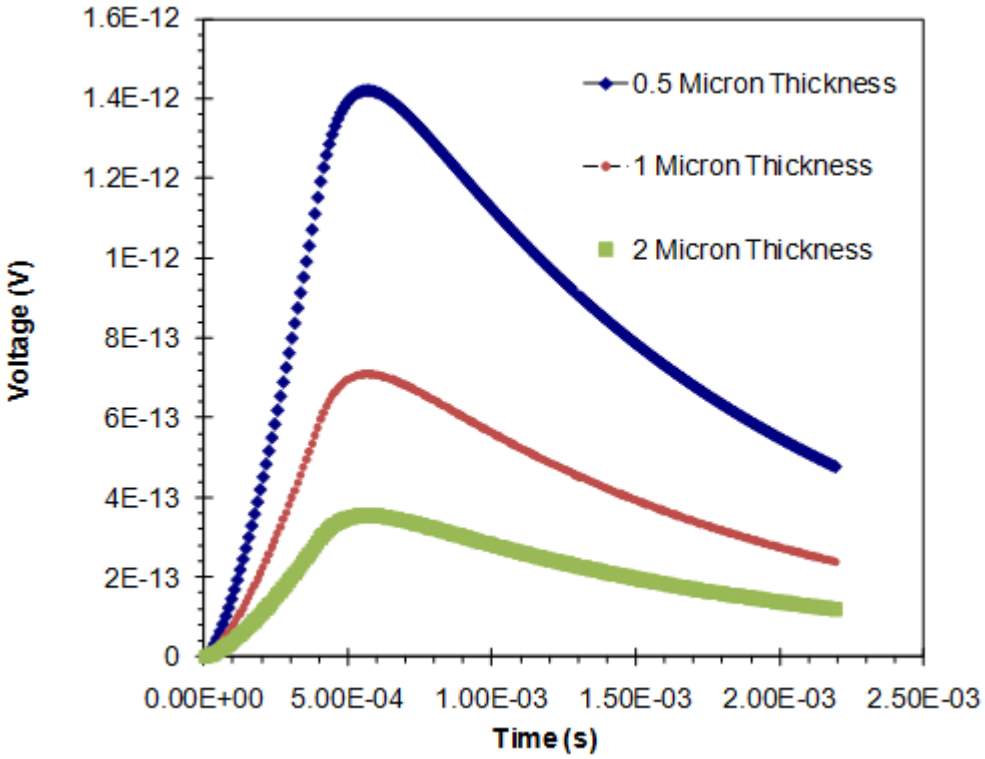

Figure 5.15: Effects of membrane geometry change

Chapter 6

Conclusions and Recommendations for Future Research

6.1 Conclusions

In this thesis, a slug flow model of droplet motion in a circular microchannel was developed, including piezoelectric membrane flexing and output voltage. The addition of this membrane allows for the thermocapillary pumping of the droplet to be converted to electricity. It was found that the net force acting on the droplet in the channel included three forces: capillary, air, and friction. The equations governing the friction, thermocapillary force and the force of air were formulated. This new force of friction was derived from a fully developed Hagen-Poiseiulle flow. It was combined with other forces to complete a new slug flow approximation for a

circular microchannel. Validation of the model was performed by comparing the predicted results against past data of Glockner.

Bending of the piezoelectric membrane was modeled as a plate. The model for bending of a circular and rectangular membrane was developed based on plate theory. It was validated by comparing two methods of bending plates. This related the piezoelectric membrane to a membrane acting as a 'plate'. The deformation of the membrane was found, then also the output voltage of the membrane. After modelling the piezoelectric effect, the predictions were compared against experimental results for the P^3 engine. The deformation results were found to be similar, but the output voltage was not identical due to different problem configurations. The model was also compared against a sample problem for piezoelectric devices, and the model was found to predict results close to the solution of the problem.

The output voltage of the micro heat engine was then studied. Initial parameters were set according to a specified configuration and material. Most of the results were found to be directly proportional to the displacement of the droplet. Various studies were performed on the original channel by varying the channel height. Various parameters were changed to study their effects on the output voltage of the system. It was found that a larger overall device would result in a larger output voltage and more cycles in less time. Different materials were studied to increase the output voltage. It was found that materials such as PZT with large

piezoelectric constants were preferable. The width of the membrane also has importance since a larger membrane results in a larger output voltage. However, a change in the length does not increase its value.

In conclusion, it was found that the voltage is directly proportional to the channel height and membrane thickness. Given a small height, there is an increase in voltage with an increase in cycle time. Likewise, a thinner membrane results in a larger voltage and increased cycle time. The material properties also play a role in the open circuit voltage of the system. Choosing a material with a high coupling factor allows the system to convert energy more efficiently, increasing the output voltage. Overall, the results provided good evidence for promising performance of the micro heat engine.

6.2 Recommendations for Future Research

The micro heat engine in this thesis has extended past developments for a rectangular closed micrchannel. The phenomenon of piezoelectricity has been discussed, studied, and applied to the system, but an optimal configuration and better performing system should be studied further, as well as experimental data to verify the predictions.

At this time, the micro heat engine outputs are low compared to the amount of heat supplied. Future work should be performed to improve the voltage output with a given amount of heat input.

This thesis explored the direct piezoelectric effect and the output voltage based on the applied stress. Additionally, research should be performed to improve the configuration of the electrical circuit and the materials used to improve the performance of the system. The study in this thesis concerned the electrodes attached to the PZT. An alernate configuration of the electrodes and placement of the piezoelectric membrane may yield improved results, so this is also recommended for future research.

The direct piezoelectric effect was added to harness the thermocapillary pumping of the microchannel. A complete system would also need to include circuitry and how the output voltage can be harnessed as usable energy, whether it is a battery or other device.

After simulating results and obtaining values based on one configuration, it is visible that the geometries of the system play a key role. It is recommended that future work be done on optimizing the system as a whole. This thesis investigated the potential of the micro heat engine under limited simulation. Work should be completed to find an optimal solution to interact between certain models such as the relationship between the slug flow approximation model and the membrane flexure

model. In this way, it may be possible to make improvements to the efficiency of the system.

References

[1] MEMSnet. *What is MEMS technology?* [Online]
Available at: http://www.MEMSnet.org/MEMS/what-is.html

[Accessed 30 June 2009].

[2] DigitTimes. *Consumer, wireless MEMS market set to grow amid downturn, says iSuppli.*[Online]
Availabe at: http://www.digitimes.com/news/a20090716PR200.html

[Accessed 27 July 2009].

[3] Lin, G., Palmer, R.E., Pister, K.S.J., & Roos, K.P. (2001). Miniature heart cell force transducer system implemented in MEMS technology. *IEEE Transactions on Biomedical Engineering*, *48*(9), 996-1006.

[4] Voskerician, G., Shive, M.S., Shawgo, R.S., Recum, H., Anderson, J.M., Cima, M.J., & Langer, R. (2003). Biocompatibility and biofouling of MEMS drug delivery devices. *Biomaterials*, *24*(10), 1959-1967.

[5] Aggarwal, P., Kaler, K.V.I.V., & Badawy, W. (2003). Design and implementation of MEMS based micro-needles for biomedical applications. *Electrical and Computer Engineering, 2003. IEEE CCECE 2003. Canadian Conference on Electrical and Computer Engineering , 3*(4), 1505-1508.

[6] Yole Developpment. *MEMS ACCelerometer, Gyroscope and IMU Market 2008-2013.*[Online]

Available at: http://www.yole.fr/pagesAn/products/MEMS_Accelerometer_Gyroscope_IMU_Market.asp [Accessed 27 July 2009]

[7] Liu, C. (2006). Foundation of MEMs. Upper Saddle River, New Jersey: Pearson Education Inc.

[8] Ericka, M., Vasic, D., Costa, F., & Poulain, G. (2005). Predictive energy harvesting from mechanical vibration using a circular piezoelectric membrane. *2005 IEEE Ultrasonics Symposium*, *2*(18), 946-949.

[9] Cui, Q., Liu, C., & Zha, X.F. (2008). Modeling and numerical analysis of a circular piezoelectric actuator for valveless micropumps. *Journal of Intelligent Material Systems and Structures*, *19*(10), 1195-1205.

[10] Zhang, S., Wang, J., & Guo, Z. (2005). Novel micro free-piston swing engine and its feasibility validation. *Tsinghua Science and Technology*, *10*(3), 381-386.

[11] Zhu, L., Lin, K.Y., Morgan, R.D., Swaminathan, V.V., Kim, H.S., Gurau, B., Kim, D., Bae, B., Masel, R.I., & Shannon, M.A. (2008). Integrated micro-power source based on a micro-silicon fuel cell and a micro eletromechanical system hydrogen generator. *Journal of Power Sources*, *185*(2), 1305-1310.

[12] Weiss, L.W. (2009). Resonant operation and cycle work from a MEMS-based micro-heat engine. *Microsystem Technologies*, *15*(3), 485-492.

[13] Chen, S., Wang, G., & Chien, M. (2006). Analytical modeling of piezoelectric vibration-induced micro power generator. *Mechatronics*, *16*(7), 379-387.

[14] Lee, E., & Wilson, T.L. (2001). A micro power supply for space micro-electromechanical systems using a high-yemperature superconductor-magnet bearing. *Nanotechnology 2001*, 477-482.

[15] Etezadi-Amoli, M., & Choma, K. (2001). Electrical performance characteristics of a new micro-yurbine generator. *Power Engineering Society Winter Meeting, Columbus, OH, 2001,* 736-740.

[16] Jeon, Y.B., Sood, R., Jeong, J.-h., & Kim, S.-G. (2005). MEMS power generator with transverse mode thin film PZT. *Sensors and Actuators A: Physical*, *122*(1), 16-22.

[17] Yang, W.M., Chou, S.K., Shu, C., Xue, H., & Li, Z.W. (2004). Development of a prototype micro-thermophotovoltaic power generator. *Journal of Physics D: Applied Physics*, *37*(7), 1017-1020.

[18] Kang, J., Kim, H., Kim, J., & Kim, T. (2002). Optimal design of piezoelectric cantilever for a micro power generator with microbubble. *2nd Annual International IEEE-EMB Special Topic Conference on Microtechnologies in Medicine & Biology,* 424-427.

[19] Miao, P., Mitcheson, P.D., Holmes, A.S., Yeatman, E.M., Green, T.C., & Stark, B.H. (2006). MEMS inertial power generators for biomedical applications. *Microsystem Technologies*, *12*(10-11), 1079-1083.

[20] Jiang, K.C., Yang, H., & Prewett, P.D. (2001). Design and analysis of a micro reciprocating engine for the time multiplexed deep etching process. *Microelectromechanical Systems Conference, Berkeley, CA, 2001,* 87-90.

[21] Hajati, A., & Kim, S.-G. (2008). Rectifier-less piezoelectric micro power generator. *Proceedings of SPIE, San Diego, California, 6928,* 1-11.

[22] Ono, Y., Mohamed, D., Kobayashi, M., & Jen, C.-K. (2008). Piezoelectric membrane sensor and technique for breathing monitoring. *Ultrasonics Symposium, Beijing, 2008. IUS 2008. IEEE*, 795-798.

[23] Wu, M., Hua, J., & Kumar, K. (2005). An improved micro-combustor design for micro gas turbine engine and numerical analysis. *Journal of Micromechanics and Microengineering*, *15*(10), 1817-1823.

[24] Piechna, J.R. (2006). Feasibility study of the wave disk micro-engine operation. *Journal of Micromechanics and Microengineering, 16*(9), S270-S281.

[25] Beeby, S.P., Torah, R.N., Tudor M.J., Glynne-Jones, P., O'Donnell, T., Saha, C.R., & Roy, S. (2007). A micro electromagnetic generator for vibration energy harvesting. *Journal of Micromechanics and Microengineering, 17*(7), 1257-1265.

[26] Bardaweel, H.K., Anderson, M.J., Richards, R.F., & Richards, C.D. (2008). Optimization of the dynamic and thermal performance of a resonant micro heat engine. *Journal of Micromechanics and Microengineering. 18*(10), 1-10.

[27] Zhang, C., Najafi, K., Bernal, L.P., & Washabaugh P.D. (2003). Micro combustion-thermionic power generation: feasibility, design and initial results. *12th International Conference on Transducers, Solid-State Sensors, Actuators and Microsystems, 1*, 40-44.

[28] Lee, C.H., Jiang, K.C., Jin, P., & Prewett, P.D. (2004). Design and fabrication of a micro wankel engine using MEMS technology. *Microelectronic Engineering, 73-74* (1), 529-534.

[29] Martinez-Quijada, J., & Chowdhury, S. (2008). A two-stator MEMS power generator for cardiac pacemakers. *IEEE International Symposium on Circuits and Systems, Seattle, WA,* 161-164.

[30] Toriyama, T., Yajima, M., & Suglyama, S. (2001). Thermoelectric micro power generator utilizing self-standing polysilicon-metal yhermopile. *14th IEEE International Conference on Micro Electro Mechanical Systems,* 562-565.

[31] Mitcheson, P.D., Miao, P., Stark, B.H., Yeatman, E.M., Holmes, A.S., & Green, T.C. (2004). MEMS electrostatic micropower generator for low frequency operation. *Sensors and Actuators A: Physical*, *115* (2-3), 523-529.

[32] Carotenuto, R., Lamberti, N., Iula, A., & Pappalardo, M. (1997). A low voltage piezoelectric micromotor using a thin circular membrane. *IEEE Ultrasonics Symposium*, *1,* 450-462.

[33] Sari, I., Blakan, T., & Kulah, H. (2008). A micro power generator with planar coils on parylene cantilevers. *Research in Microelectronics and Electronics,* 133-136.

[34] Kulah, H., & Najafi, K. (2004). An electromagnetic micro power generator for low-frequency environmental vibrations. *17th IEEE International Conference on Micro Electro Mechanical System*, 237-240.

[35] Lu, F., Lee, H.P., & Lim, S.P. (2004). Modeling and analysis of micro piezoelectric power generators for micro-electromechanical-systems applications. *Smart Materials and Structures*, *13* (1), 57-63.

[36] Whalen, S., Thompson, M., Bahr, D., Richards, C., & Richards, R. (2003). Design, fabrication and testing of the P^3 micro heat engine. *Sensors and Actuators A: Physical*, *104*(3), 290-298.

[37] Beeby, S., Ensell, G., Kraft, M., & White, N. (2004). MEMS Mechanical Sensors. Norwood, MA: Artech House.

[38] Solecki, R., & Conant, R.J. (2003). Advanced mechanics of materials. New York, NY: Oxford University Press.

[39] Van Rijn, C.J.M. (2004). Nano and micro engineered membrane technology. Amsterdam, The Netherlands: Elsevier B.V.

[40] Elwenspoek, M., & Wiegerink R. (2001). Mechanical microsensors. Berlin, Germany: Springer-Verlag.

[41] Chen, W.F., &Lui, E.M. (2005). Handbook of structural engineering. (2^{nd} ed.). Boca Ration, Florida: CRC Press.

[42] Hearn, E.J. (1997). Mechanics of materials 2 (3^{rd} ed). Woburn, MA: Butterworth-Heinemann.

[43] Yang, J. (2005). An introduction to the theory of piezoelectricity. New York, NY: Springer Science + Business Media Inc.

[44] Bao, M. (2005). Analysis and design principles of MEMS devices. Amsterdam, The Netherlands: Elsevier B.V.

[45] Armenakas, A.E. (2006). Advanced mechanics of materials and applied elasticity. Boca Raton, FL: Taylor and Franics Group

[46] Ventsel, E. & Krauthammer, T. (2001). Thin plates and shells – theory, analysis and applications. New York, NY: Marcel Dekker, Inc.

[47] Timoshenko, S., & Woinowsky-Krieger, S. (1959). Theory of plates and shells. United States of America: McGraw-Hill Book Company, Inc.

[48] Glockner, P.S. (2006). Numerical and experimental investigation of thermocapillary pumping in closed-end microchannels for micro heat engines. University of Manitoba. Winnipeg, Manitoba, Canada.

[49] Kundu, P. K., Cohen, I. M., Ayyaswamy, P. S., Hu, H. H. (2007). Fluid Mechanics (4th ed). Burlington, MA: Academic Press.

[50] Sodano, H. A., Inman, D. J., Park, G. (2005). Comparison of piezoelectric energy harvesting devices for recharging batteries. *Journal of Intelligent Material Systems and Structures*, 16 (10), 799-807.